NTNU

Norwegian University of
Science and Technology

Non-Linear Finite Element Analysis of Sheets with Integrated Patterns

Identification of the Significant Mechanisms
contributing to Non-Linear Behavior

Eivind Lystad Grimstad

Master of Science in Mechanical Engineering
Submission date: June 2018
Supervisor: Nils Petter Vedvik, MTP
Co-supervisor: Martin Steinert, MTP

Norwegian University of Science and Technology
Department of Mechanical and Industrial Engineering

Preface

This report is a Master's thesis at Department of Mechanical and Industrial Engineering (MTP) Gløshaugen. The work has been carried out during the spring semester of 2018. It is a continuation of a project report written in the previous semester by Oddvin Østmo, Stian Birkeland and Eivind Lystad Grimstad, on *flexure patterns*. The idea to the current wok was brought up in collaboration with the supervisor, and can be seen as a natural extension on the named topic.

The results from this report is aimed at designers working with, and exploring, new design methods, surface materials and compliant mechanisms. The reader is assumed to be familiar with basic mechanics, but the relevant theory will be explained wherever needed.

June 11, 2018
Eivind Lystad Grimstad

Acknowledgment

I would like to thank my supervisor Nils Petter Vedvik, for relentless guidance throughout this semester, giving me strategical advice as well as motivation and theoretical insight. I also want to thank Oddvin Østmo, for bouncing of ideas and good feedback.

E.L.G.

Abstract

By cutting specific patterns in thin sheets of material it is possible to acquire a high degree of compliance in and out of the plane. These structures, called *flexure patterns*, are often applied in situations causing large deformations and contact. This is known from theory to introduce a non-linear behavior, in which the load and deformation no longer has a linear relation.

This thesis sets out to analyze these sources of non-linearity, and find their significance in design applications. This is done by performing a parametric study of the *base repeating unit* of two known patterns: the *LET/Slits* pattern and the *YdX*. The goal is to contribute to the knowledge and understanding of the mechanical behaviour of flexure patterns. Non-linear simulations with the FE-software ABAQUS have been used in combination with python to make the analyses as automatic as possible.

The results show that for some load cases there are small deviation between the linear and the non-linear simulation. The deformation mechanisms of important structural members are assumed to play significant roles as sources of geometric non-linearities. In addition, the results indicate that an automatic analysis of contact non-linearities would require further work and is a complete study by its own.

Samandrag

Ved å kutte spesifikke mønster i tynne plater, er det mogleg å få ei høg grad av responsiv deformasjon i, og ut av planet. Desse strukturane, kalla *flexure patterns*, stettar bruksområde der store deformasjonar og kontakt er venta. Frå teorien, er dette kjent for å føre til ikkje-lineær åtferd, der last og deformasjon ikkje har ein lineær samanheng.

Denne oppgåva gjev seg ut på å analysere kjeldene til desse ikkje-lineæritetane, of avdekke kor stor innverknad dei har i design-bruksområde. Dette har blitt gjort ved å gjere ei parametrisk studie av den repeterande einingscella, eller *base repeating unit*, av to kjende møster: *LET-/Spaltemønsteret* og *YdX*. Målet er å bidrage til kunnskapen og forståinga av den mekaniske åtferda til *flexure patterns*. Ikkje-lineære simuleringar med FE-programvare i ABAQUS har blitt nytta saman med koding i Python for å gjere analysene så automatiske som mogleg.

Resultata viser at for somme lasttilfelle er der lite avvik mellom den lineære og ikkje-lineære simuleringa. Deformasjonssekvensane for sentrale element i strukturen er vert sett på som avgjernade kjelder til geometrisk ikkje-lineæritet. I tillegg indikerer resultata at ei automatisk ikkje-lineær kontaktanalyse krevjer meir arbeid, og at det er eit studie i seg sjølv.

Contents

List of Figures

List of Tables

1 Introduction

This thesis deals with the phenomenon non-linearity in structures, specifically in sheets and plates with integrated patterns. The patterns in question is cut all the way through the thickness of the plate and could give the material a high degree of flexibility, opening up for a range of new applications - thus making this an interesting topic to study. In the project work [5] written in the fall 2017, different patterns were explored and the main mechanisms of motion and deflections were identified, in order to categorize and define each structure. Models in ABAQUS and physical test specimens were compared and analyzed with the help of common mechanics of thin sheets. The results indicated a transition from the linear to the non-linear regime, which potentially could be of great significance to designers and engineers working with these new flexible materials.

Rooting from the project thesis and the knowledge acquired on flexure patterns, this work sets out to investigate the non-linearities associated with these mechanisms, and tries to find their significance in practical applications. The problem statement for the thesis is as follows:

> The mechanical behavior of sheets and plates can be severely modified by patterns cut through the sheet serving as a precursor. The modified structure may find many new applications where specific tailor-made flexibility is desired. Such structures may also serve as various mechanisms in mechanical systems. The principal mechanical behavior has previously been described in a linear framework by adopting the relations for thin shells through a shell stiffness matrix. For many situations it is, however, expected that a useful approach would need to include non-linear effects. The current work will study the various sources of non-linearity, including material non-linearity, large deformations and contact.

There has not been performed a quantitative non-linear study of patterns on this kind, so a starting point was chosen for fundamental cases with a limited number of patterns.

A part of the task was also to specify the problem statement by the following objectives an limitations:

Objectives:

- General objective: Contribute to the knowledge and understanding of the mechanical behavior of flexure patterns
- Specific objective: Assessing the significance of non-linear behavior by performing a quantitative non-linear parametric study on selected flexure patterns
- Automate the process of the parametric study by ABAQUS scripting in python

Limitations:

- The study was limited to two principal patterns: Slits and YdX
- Geometrical non-linearities due to large deformations and contact are included in the numerical study, while effects of material non-linearity are only qualitatively described
- An identical set of elastic properties are being used for all numerical cases since a

variation of these properties is primarily reduced to a simple scaling effect, du to the proportionality of the structural stiffness

- Only materials with isotropic properties have been considered

The first chapters of this report summarize the definitions and findings presented in the project work prior to this study, with the intention of giving the correct context of the research. A theory chapter presents the theory used, giving a reference guide while reading the thesis, and then a section presenting the relevant literature and concepts. The work method and approach are presented in the method chapter. As there probably are several ways to do a non-linear research, a proper presentation is to be expected. In addition, some additional limitations and presumptions will be discussed and set. The last part of the thesis gives an objective presentation of the results from each analysis, followed up by the respective discussion on how they could be interpreted. In the end comes a conclusion giving a short summary of the findings and useful insights emerging from the work, in addition to improvements, further work and how this research could be used.

2 Background - the project work

The goal of the project work [5] was to explore the concept of living hinges, or *flexure patterns* - a way to increase the compliance of a sheet of material. This exploration was done in a typical wayfaring model [6], with little base knowledge about the topic at hand. In addition to information gathering, these were the bullet points:

- Establish a proper definition of a flexure pattern described in terms of symmetry groups and flexure mechanisms.
- Describe the properties of the flexure pattern in terms of plate theory.
- Compare different calculation models and their applicability to flexure patterns.
- Conduct physical tests.
- Explore new possibilities and applications.

The following sections are extracted from the project and commented on wherever additional context is necessary.

2.1 Project Abstract

A flexure is a flexible element that can withstand large deflections. By combining multiple flexures in a plane, a flexure pattern can make a plate able to withstand relatively large deformations without deforming plastically. The advantages of using flexures are primary related to compact design and reduced need of assembly.

This project presents a new definition of flexure patterns where symmetry and wallpaper group theory is related to the flexure mechanisms. From this, several new patterns that show interesting behaviour are created and discussed.

A short study of laser cutting as a manufacturing process for making flexure patterns is conducted. Other promising manufacturing processes are also presented.

A generative unit is used analytically and by finite element analysis to obtain values for the stiffness matrix components. The analytic methods models one type of flexure patterns as springs to obtain two stiffness components. It is further shown how springs are used to model more complicated patterns.

The analytic expressions model the unit as too stiff compared to the finite element analysis, while the bending testing generally underestimates the values. The analytic expressions and finite element analysis can be improved by including nonlinear behaviour. The bend testing shows promise, but could improve from using standardized testing equipment. The twist bending test shows a useful way of collecting displacement and force data. The expression for obtaining the material stiffness needs, however, further work to give good results.

2.2 Flexure patterns

Rigid body mechanism

The definition used in this project is a mechanical device that transfer or transforms motion, force or energy. [7] The traditional rigid body mechanisms consists of rigid links connected at movable joints. Joints can be considered the heart of a rigid body mech-

anism; they are defined as kinematic pair of connection between to bodies that impose constraints on their relative movement.

Orthoplanar mechanisms

Orthoplanar mechanisms, as seen in figure 1 have joints in-plane for a compact state, but the movement of the mechanism is out of plane. The advantage of these mechanisms is their compressed state combined with their movement [8].

Figure 1: An orthoplanar spring from [1].

Their disadvantages is that they are *change-point mechanisms*, meaning that they are bi-stable. There exists a point in the deformation where it has a potential of changing into two possible configurations of movement.

Compliant mechanism

Compliant mechanisms primarily gain their flexibility from the deflection of flexible elements rather than a movable joint. Compliant mechanisms are advantageous since they can reduce the part count, thus reducing cost and assembly time. The reduced part count can also increase the precision of the mechanism since it does not require a number of other parts to fulfill their dimension requirement.

For simplified designs, designers often make use of compliant mechanisms due to their reduced part count. Precision instruments are also suitable for compliant mechanisms, as they rely on as little backlash as possible.

Fully-compliant mechanisms are mechanisms that *only* consists of flexible members.

Metamorphic mechanisms

A metamorphic mechanism is a mechanism that can change its mechanical behaviour by doing specific motions or entering specific configurations.

A typical example is an *erectable metamorphic mechanism*, or the flat cardboard box which can be put into a rigid state.

Contact-aided mechanisms change their movement by introducing additional stiffness from having restricting links.

Flexure

A *flexure*, is the term for a flexible element, or a combination of such elements, that can be engineered to be compliant in specific degree of freedom. In solid mechanics the primary deformation mechanisms of concern are bending, torsion, shear, elongation and compression. The amount of deformation is controlled by the geometry of the beams as well as the material. For basic elements like cantilever beams or for plates made from a stiff materials, large travel distances are only achieved by bending and torsion. There

are three main types: The *pin flexure* is a bar, or a cylinder of material with, a notch cutoff and 3 degrees of freedom; the *blade flexure* has 4 degrees of freedom; and the *notch flexure* has 5 degrees of freedom. The three are shown in figure 2a, 2b and 2c. A flexure that is compliant only in one rotational degree of freedom is often called a *flexure bearing*.

A linear flexure bearing is restricted only to one translative degree of freedom. Since single flexure features are limited in both travel capability and degree of freedom, *compound flexure systems* are designed using combinations of the component flexure features mentioned above. Using compound flexures and complex motion profiles with specific degrees of freedom, relative long travel distances are possible for compliant mechanisms.

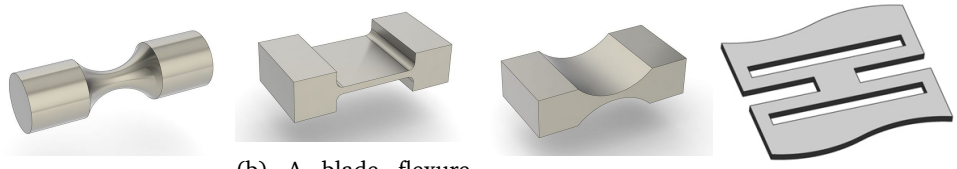

(a) A pin flexure with 3 degrees of freedom. Three rotational

(b) A blade flexure with 2 degrees of freedom. One translative, and one rotational.

(c) A notch flexure with 1 degree of freedom. One rotational.

(d) A laminar emerging torsional (LET) joint.

Figure 2: The differnet flexures

Lamina emergent mechanisms

Lamina emergent mechanisms (LEMs) are classified as ortho-planar compliant mechanisms. They replace traditional joints, hinges and mechanisms and can have advantages in size, manufacturing sensitivity and have less unwanted motion in trade-of with the time used to design the mechansims. The mechanical behaviour of these have been defined for the case of a single mechanism [9] and when replicated in an array [10].

Names for joints and flexures

There exists a variety of names for different types of rigid body joints or flexures, depending on their respective geometry, deformation mechanisms and manufacturing processes. The names varies from being well defined in scientific literature, to being trivially defined on internet forums. Some examples are: torsional hinge, cross axis flexural pivot, living hinge seen in figure 3a, kerf bend in figure 3b, parallelogram joint, deltoid joint, leaf spring, lamina emergent torsion joint as in figure 2d and lattice hinge.

Oddvin Østmo further refined the definition on the flexure pattern in his own master thesis, spring 2018. The broad definition is found in the appendix, part C A.2, but the specific one is as follows:

Flexure pattern is characterized as a 2 dimensional metamaterial that consists of flexures configured in a pattern that increase the compliance compared to the bulk material. The flexures are patterned onto the plane according to a set of rules.

2.3 Auxetic behaviour

Auxetic behaviour

One of the elastic properties of a material is the Poisson's ratio. This constant tells something about how a material deforms transversely when loaded in the longitudinal direc-

(a) A flexure from a food container made from plastic. Often referenced to as a living hinge.

(b) Kerf bend is a kind of flexure usually made with subtractive manufacturing in wood.

Figure 3: Examples of names used on different flexure applications

tion. Stretching of a material with a *negative Poisson ratio*, causes it to become thicker perpendicular to the applied force.

Materials or structures that show the unusual property of having a negative Poisson ratio are called auxetic. Evans et. al. writes that the Poisson ratio has historically been the least studied of the four elastic constants for isotropic materials [11]. In their paper they list different auxetic structures found in both nature and in man-made products, on a microscopic and macroscopic scale. As flexure patterns can be auxetic, it is an interesting potenital.

An auxetic property is achieved by introducing a specific pattern to the structure. A very common pattern is the re-entrant honeycomb pattern seen in figure 4a. Re-entrant means pointing inwards, and could be used to describe a pattern that have been reoriented in a way so that it folds inwards. In this case, the ordinary honeycomb pattern shown in figure 4, has been re-entered. In resent years, application study of auxetic materials have increased, and scientists are constantly searching for more patterns that have auxetic properties. An example of one of these search methods are given in by Korner and Liebold-Ribeiro [12]. They use the eigenmodes of the basic shapes quadrat, triangle and hexagonal, to identify new auxetic shapes. The re-entrant honeycomb pattern was identified with this method.

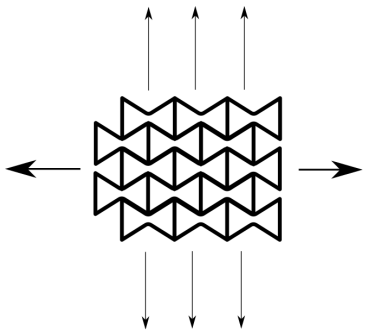

(a) Re-entrant

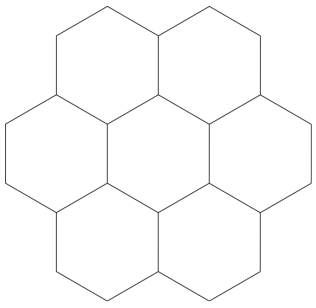

(b) Normal

Figure 4: Two forms of the honeycomb pattern

Evans et al.[11] mentions that auxetic patterns have *synclastic curvature* property. This is also referred to as having positive Gaussian curvature, and means that the plate can achieve double curvatures like dome shapes. Examples of anticlastic and synclastic

curvature is shown in figure 5.

Figure 5: l. Anticlastic/positive Poisson ratio, r. Synclastic/negative Poisson ratio

In this project the method used to explore auxetics was to produce different patterns and conform them to a domed shape. In addition, the patterns were stretched in one direction. By visual measurement, it was observed how the cross-sectional width changed. In most cases the width shrank, but there was some patterns that showed a negative Poisson ratio. A tactile study of the different patterns was also performed, due to the counter-intuitive way these materials deform.

Considering the possible applicatons for auxetic patterns; Konakovic et al. [2] uses a triangular auxetic pattern in combination with *conformal mapping* to produce 3D modelled shapes. Konakovic et al. uses different metals for his patterns, but in this project a fairly porous wood based material was used (MDF). The chosen auxetic patterns produced from MDF were either too stiff or failed easily. An explanation is that since the primary motion of a auxetic behaviour is rotation [12], it is required that the material can have plastic deformation in connecting points, without causing any fracture in the material. MDF is believed to have a poor ductility. The same auxetic pattern that Konakovic used was produced in MDF, as seen in figure 6. The links fractured without much effort.

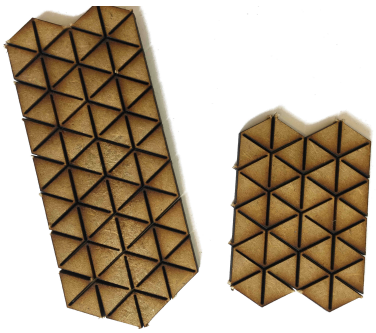

Figure 6: Auxetic triangle pattern like the one used in Konacovics paper [2], made of MDF

The knowledge of auxetic materials and how they behave led to some discoveries on the flexure patterns that had already been used. The best example of this is the YdX, used in several of the other studies. It showed to have a negative Poisson ratio when subjected to tensile loads. A closer look at the pattern revealed that it was in fact a slightly modified version of the re-entrant honeycomb, shown in figure 7.

2.4 Material constants for MDF

Some initial tests was performed with MDF dogbones, to determine the material properties of the base material used to make the patterns. A standard tensile test was conducted

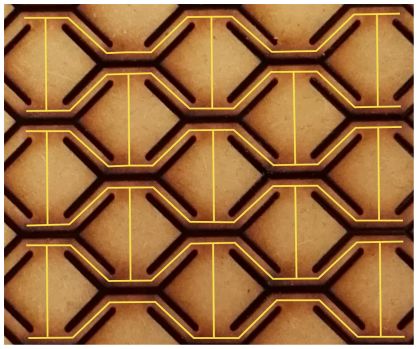

Figure 7: The YdX pattern with the modified re-entrant honeycomb pattern drawn for visualization

on specimens cut out with the laser cutter. The dogbones had a reduced area with the dimensions: length, 164 mm; width, 14 mm; thickness, 3mm. The strain rate was 1 mm/min.

Figure 8: The two perpendicular strain gauges.

Two strain gauges was placed perpendicular to each other in order to get the Poisson's' ratio which can be calculated by equation 2.1.

$$\nu_P = -\frac{\text{Lateral strain}}{\text{Axial strain}} = -\frac{\varepsilon_L}{\varepsilon_a} \tag{2.1}$$

From the data obtained, two interesting curves can be plotted, longitudinal strain versus axial strain, seen in figure 9a and stress versus strain, seen in 9b.

Results

We can see the curves has a linear relationship in the beginning of the test. The material shows signs of weakening above 10 MPa, where a non-linear relationship is getting dominant. The derived material constants is seen in table 1.

Table 1: Material constants for 3mm MDF plate

Youngs modulus	Poisson ratio	Elongation	Ultimate tensile strength
3690 MPa	0.24	1.87 %EL	21.5 MPa

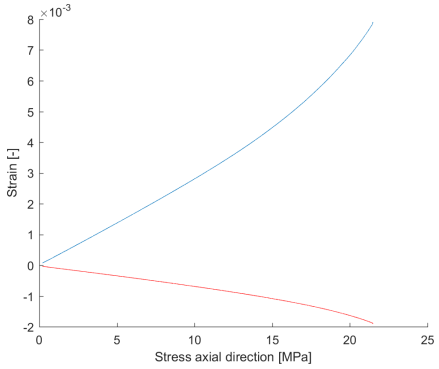

(a) Longitudinal and lateral strain versus axial stress.

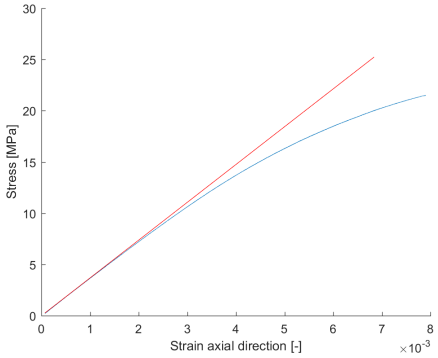

(b) Stress versus strain. linear response plotted is red line.

Discussion

MDF is not a consistent material and the assumption of isotropy is probably not realistic. It consists of a mix of random oriented viscose fibers in a matrix of lignin, polymers, glue and probably other unknown substances. Because of the random orientation and short fibers, the MDF can be assumed to be transverse isotropic. The fracture surface showed signs of delamination, which is a sign variable strength across the thickness.

The non-linear effects are assumed to be results of plasticity, relaxation, creep or other non-linear effects in the material.

The strain gauges could potentially be affected by a temperature change in the environment due to thermal expansion. This was not taken into consideration, but since the tests were done in room temperature it was assumed neglected.

2.5 Tensile test of YdX

Introduction

This section explores the possibility to acquire the stiffness of a flexure pattern by the use of conventional tensile testing. The pattern used is the standard YdX. The stiffness matrix components in question is the A_{yy} in the direction of the load. The results obtained is compared to a FEA simulation.

Theory

In the case of the flexure pattern that were tensile tested, the constitutive equations for symmetric laminates, given in eq. 2.2, were applied. This theory is based on pure tension of plates where, in this case, there is a prescribed displacement control load only in the y-direction.

$$\begin{bmatrix} N_x \\ N_y \\ N_{xy} \end{bmatrix} = \begin{bmatrix} A_{xx} & A_{xy} & 0 \\ A_{xy} & A_{yy} & 0 \\ 0 & 0 & A_{ss} \end{bmatrix} \begin{bmatrix} 0 \\ \varepsilon_y \\ 0 \end{bmatrix} \tag{2.2}$$

Method

A clamping mechanism was made to attach the specimens to the tensile machine. They were made from sheets of metal 3mm thick, with bolts going through them to tighten the clamping, as seen in figure 10.

Two identical YdX patterns were tested, and both were oriented the same way. This

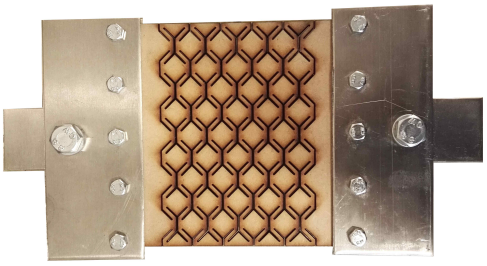

Figure 10: The prototype of the tension test fasteners.

would show if the failure mechanisms seemed to be similar for both the specimens.

The rate of displacement was 1mm per minute.

A duplicate of the YdX part was modelled in Abaqus. The boundary conditions were made to simulate the real condition. This meant total fixture at the upper and lower edge. A displacement of 9.9 was applied to the structure, similar to the physical test.

Results

The raw data from the tests showed some anomalies in the first seconds of the test. This was assumed to come from instability of the clamping mechanism. Normal practice is to neglect the first part of a tensile test to give the equipment time to stabilize itself.

The data from the testing machine was given as load force versus strain, and are displayed in figure 11.

The A_{yy} values were calculated with the formula $A_{yy} = \Delta N_y / \Delta \varepsilon_y$ and are listed in table 2. The ΔN_y and $\Delta \varepsilon_y$ was used because a single strain value from the graph would contain all the accumulated errors from the previous values.

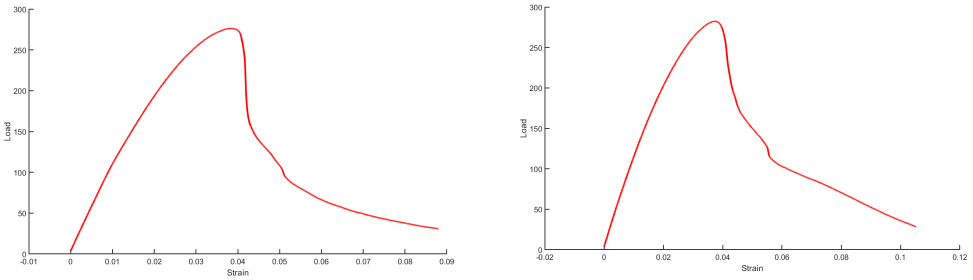

(a) Load-Strain, YdX1

(b) Load-Strain, YdX2

Figure 11: The resulting plots from the tensile test of YdX

The FE-analysis of the YdX pattern gave some interesting results. The resultant forces were distributed at the upper part of the structure as seen in 12, with a total magnitude of 1295.8N. The width of the plate was 142.6, thus the normalized force was $N_x = 9.0869 N/m$. Using the equations given in section 3.1 gave $Ayy = 89.880$.

In figure 13 the simulation model and the physical part of the YdX pattern are displayed.

Table 2: A_{yy} results

Test	Specimen type	Specimen cross section [mm]	A_{yy}
1	Rectangular YdX	140.7x 3	84.5798
2	Rectangular YdX	140.7x3	79.7169

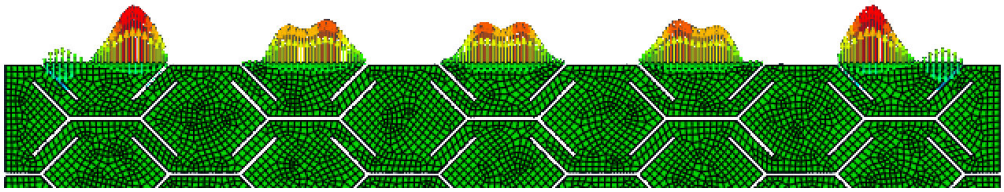

Figure 12: The distribution of the resultant forces

Discussion

The clamps constrained the flexure pattern in the x-direction at the top and bottom. This lead to resultant forces in the x-direction producing the normalized force N_{xx}, which again gave contribution to the A_{xx} stiffness component. This means that the calculated stiffness's listed in table 2 have an error. For this reason, the only way to get the correct value of A_{yy} is to run a simulation with no boundary condition in Abaqus. The values are however approximately the same as the values produced from the Abaqus analysis, when the boundary conditions in the simulation were set equal to the physical test. Even the deformation procedure seems to be quite similar; figure 14 shows the same corner for both the FEA and the physical test, and the boundary constraint causes the pattern unit to deflect outwards. In figure 13 the physical piece does not bulge at the sides as the Abaqus model does, but this is due to its unloaded state. In tension it had a much wider middle cross section. Another important note about the differences between simulated and the physical test is that the latter has been subjected to large geometric non-linearities from the deformations, while the other one shows only elastic behaviour.

Further work

The boundary condition at the fixed ends of the test pieces introduced an error when calculating the $A_{y}y$. This means that the current test rig is not applicable for giving the

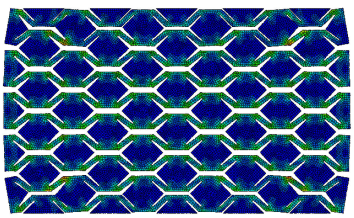

(a) FEA

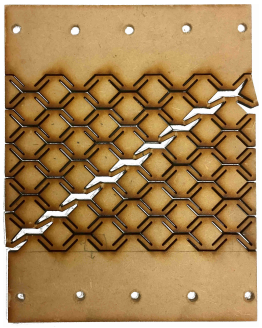

(b) Physical

Figure 13: The whole YdX specimen

(a) FEA

(b) Physical

Figure 14: Detail of edge effect on specimen

real stiffness of the pattern. A further improvement of the test rig could be to add a degree of freedom in the x-direction. Some early stage thoughts on how to do this is shown in figure 15, where the attachment points of the pattern is able to expand in horizontally.

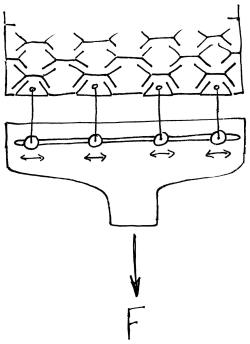

Figure 15: Sketch on improvement of tensile test

During the whole test the specimen was recorded, to document its deformation. A future test rig would also have an improved measurement technique. DIC(Digital Image Correlation) is one such method. By finding the relative displacement between specific points on the pattern, the strain in all the y- and x-directions could be calculated, and thus give the full plain strain stiffness matrix.

2.6 Cylindrical bending test

Application of plate theory

The core principle of the test is to apply a equal amount of moment on each end to approximately have an constant curvature throughout the length. This allows simple calculations of the bending moment stiffness components

$$\begin{bmatrix} M_{xx} \\ M_{yy} \end{bmatrix} = \begin{bmatrix} D_{xx} & D_{xy} \\ D_{xy} & D_{yy} \end{bmatrix} \begin{bmatrix} \kappa_{xx} \\ \kappa_{yy} \end{bmatrix} \tag{2.3}$$

or in terms of compliance,

$$\begin{bmatrix} \kappa_{xx} \\ \kappa_{yy} \end{bmatrix} = \begin{bmatrix} d_{xx} & d_{xy} \\ d_{xy} & d_{yy} \end{bmatrix} \begin{bmatrix} M_{xx} \\ M_{yy} \end{bmatrix} \tag{2.4}$$

where stiffness and compliance components are constants.

For testing in x-direction, a given value of M_{xx} results in κ_{xx}. If κ_{yy} is restricted, a moment M_{yy} is also present. Meaning the relation between applied moments, curvature and compliance is

$$\begin{bmatrix} \kappa_{xx} \\ 0 \end{bmatrix} = \begin{bmatrix} d_{xx} & d_{xy} \\ d_{xy} & d_{yy} \end{bmatrix} \begin{bmatrix} M_{xx} \\ M_{yy} \end{bmatrix} \tag{2.5}$$

$$\frac{\kappa_{xx}}{M_{xx}} = d_{xx} - \frac{d_{xy}^2}{d_{yy}} \tag{2.6}$$

Similarily, a given a value of κ_{xx} results in value of M_{xx}, but the displacement is not restricted by M_{yy} and the relation between applied curvature, moments and stiffness is

$$\begin{bmatrix} M_{xx} \\ 0 \end{bmatrix} = \begin{bmatrix} D_{xx} & D_{xy} \\ D_{xy} & D_{yy} \end{bmatrix} \begin{bmatrix} \kappa_{xx} \\ \kappa_{yy} \end{bmatrix} \tag{2.7}$$

$$\frac{M_{xx}}{\kappa_{xx}} = D_{xx} - \frac{D_{xy}^2}{D_{yy}} \tag{2.8}$$

To compare with values from the finite element analysis, the values of M/κ is calculated. Equations 2.6 and 2.8 show that

$$\frac{M_{xx}}{\kappa_{xx}} = \left\{ \frac{1}{d_{xx}}, D_{xx} \right\} \tag{2.9}$$

For $D_{xy} \ll D_{xx}$, equation 2.8 gives the approximate value for D_{xx}. Similar argument is made for D_{yy}.

Method

The equipment besides the built rig are **a)** weights, **b)** Arduino Uno mictrocontroller, and InvenSense MPU-6050 MEMS-gyroscope.

Since the bent plate has constant curvature throughout the length, it is a curve segment on a circle with curvature κ. By measuring the angle where the plate is fastened, the curvature can be calculated using a single sensor. The measured variable is the angle of rotation of the fastener and is measured using a gyroscope and a microcontroller. Using weights and a set distance from the rotation center, the applied moment is a discrete dependant variable on the independent variables weight and distance from rotation center. Since both curvature and moment is known, the matrix component D_{ii} can be calculated.

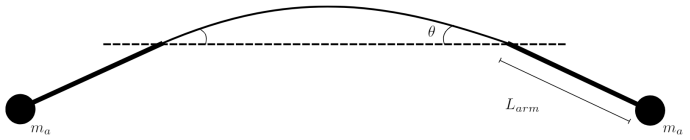

Figure 16: A concept of calculating the curvature from known values θ and S.

The purpose of the improved rig is to obtain as accurate results as possible and further detect difficulties with the testing concept. The following parameters were put in consideration when designing the rig:

Level testing conditions: The rig is built with extruded aluminum profiles for minimal error in building material dimensions. The test-rig has adjustable legs to obtain level testing conditions. The gyroscope was calibrated using a level surface.

Symmetric loading conditions: The fasteners are machined by hand to reduce error stemming from difference in dimensions and weight. Roller bearings were attached at the rotational pins to allow the distance between fasteners to retract when weight was applied. Without the roller bearings, forces N_i friction would interfere a noticeable difference.

Rotation centre: The rotation center is designed to lay in the middle of the testing specimen for plates with thickness $t = 3$ mm. For the plates with $t = 1$ mm, additional 1 mm plates were inserted to obtain wanted rotation centre.

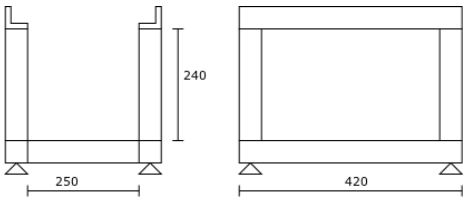

(a) Dimensions of the rig.

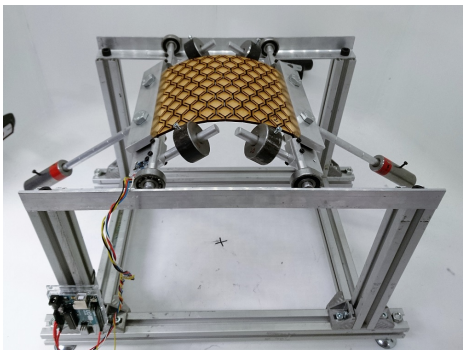

(b) Built rig with testing specimen and test.

Figure 17: The main dimensions of the rig as well as an example specimen in testing.

Test procedure

The following materials and plates were put into the testing rig and tested, see table 3.

Table 3: Specimen used for bending tests.

Plate number	Specimen type	WidthxLength [mm]	Calcualted value from test
1	MDF Rectangular YdX	136x178	Dxx
2	MDF Rectangular YdX	140x157	Dyy
3	MDF Rectangular Slits	147x163	Dyy
4	MDF Rectangular Slits	147x186	Dxx
5	MDF Rectangular Solid	147x185	D
6	316L Steel Rectangular Solid	147x150	D
7	316L Steel Rectangular Solid	153x150	D
8	MDF Rectangular Slits	143x148	Dyy
9	MDF Rectangular Slits	147x143	Dyy

Specimen type describes materials and the pattern applied to the plate, width is the width of the plate, length is the distance between the front of the fasteners and the distance of the plate that gets bent and test variable is the result that performing the test yields.

To check the accuracy and precision of the testing method, plate 6 were put into bending in four orientations with two different load cases. rotation center, see figure 16. Plate 7 from the same sheet of metal was tested at two orientations on two sides at one distance L_a. A solid $t = 3$ mm MDF plate was tested to get an indication of the

anisotrophy of MDF as material. The test results were compared to solid plate stiffness values D_m.

For plates 1-4, both sides were tested with two load cases which gives 4 results. For plate 8 and 9, the fastened ends had different pattern of removed material to test if inside or outside LET configuration at fastened ends would affect the results.

Results

Table 4: Resulting $\bar{D}_T$ from test comprared to D_m

Plate nr.	Repetitions	$\bar{D}_T$ [Nmm]	D_m [Nmm]	$\bar{D_T}/D_m$
5	4	11122	8854	1.256
6	8	16857	17155	0.983
7	2	16827	17155	0.981

Here $\bar{D}$ is the mean plate stiffness acquired from testing and D_m is base solid plate stiffness.

Table 5: Resulting $\bar{D}_{ii}$ from test.

Plate nr.	Repetitions	m_a [g]	L_a [mm]	Calculated matrix component	$\bar{D}_{ii}$ [Nmm]	D_{FE}
1	4	217	70, 250	Dxx	1377	1971
2	4	217	70, 250	Dyy	373	429
3	4	217	70, 250	Dyy	95	139
4	4	217	70, 250	Dxx	5825	5034
8	4	217	70, 250	Dyy	119	134
9	4	217	70, 250	Dyy	117	134

Table 6: Variations of D_{ii} from testing

Plate nr.	rep. 1 L_a=70mm	rep. 2 L_a=220mm	rep. 3 L_a=70mm	rep. 4 L_a=220mm	$\bar{D}_{ii}$	sample standard deviation, Sii
1	1320	1462	1278	1447	1377	80
2	342	408	339	402	373	32
3	89	104	92	96	95	6
4	5568	5836	5685	6213	5826	244

For full values of the test, see appendix **ref appendix**.

2.6.1 Discussion

Testing procedure

Error stemming from the linearity of the testing can affect the results. Multiple testings with either change in weight or arm should be done to see if the plate behaviour is within linear behaviour and randomization should be done to minmize the effect of linearity in test procedure.

For the current test results, it is not known if the rise in D_{ii} values for larger L_a is because of wrongly assumed linear relationship between curvature and moment or if it is other non-linear effects.

Creep and relaxation

As MDF is a material with visco-elastic behaviour, which means it is also effected by creep and relaxation. This was observed in the test as a small drift of the measured angle after the load was applied and stabilized and is consequently a small measurement error. This was however a small contribution compared to the measured angle, and will not affect the results in a significant way. After the tests was conducted some specimen were permanently deformed. This could be because of creep in the material and is also a source of non-linearities, which the theory presented here does not account for.

Non-linearity

Geometric non-linearities is not covered. For the testing, the specimen's stiffness is assumed constant and for small deformations this will often be true. If the beams are heavily distorted, the stiffness might not be constant.

Plastic deformation might affect the results as well. For the plates and mechanisms, stresses are not considered. Therefore there is not a known indication of when plastic deformation might occur or if it occurred in our tests.

A larger applied load gives a higher resulting stiffness, see table 6. Assuming MDF is a strain softening material, the effect of large deformations could be a non-linear geometric effect.

Contact non-linearity is attempted avoided for the physical testing. A relatively large gap was made when manufacturing the pattern to avoid contact when bended.

Boundary conditions

As mentioned initially, when the testing specimen is clamped an unwanted moment is applied, inhibiting the resulting curvature of the coupling term D_{xy}. As predicted, the tested values are lower than the finite element results would indicate.

3 Theory

3.1 The linear approach

3.1.1 Hookes law

Hookes law is an assumption for linear elastic materials and states the linear relationship between stress and strain. Voigt notation for this is $\boldsymbol{\sigma} = \mathbf{C}\boldsymbol{\varepsilon}$, where bold represents matrices. For a material with no symmetry, this relationship has to be described for each component of the stress tensor in figure 18 and is $\sigma_{ij} = C_{ijkl}\varepsilon_{kl}$ where $i, j, k, l = 1...3$ and C_{ijkl} is a 3x3x3x3 matrix with 81 constants. Due to symmetry this simplifies to $\sigma_i = C_{ij}\varepsilon_j$ where $i, j = 1...6$ and C_{ij} is a 6x6 matrix with 21 independent constants.

$$\begin{bmatrix} \sigma_1 \\ \sigma_2 \\ \sigma_3 \\ \tau_{23} \\ \tau_{13} \\ \tau_{12} \end{bmatrix} = \begin{bmatrix} C_{11} & C_{12} & C_{13} & C_{14} & C_{15} & C_{16} \\ C_{21} & C_{22} & C_{23} & C_{24} & C_{25} & C_{26} \\ C_{31} & C_{32} & C_{33} & C_{34} & C_{35} & C_{36} \\ C_{41} & C_{42} & C_{43} & C_{44} & C_{45} & C_{46} \\ C_{51} & C_{52} & C_{53} & C_{54} & C_{55} & C_{56} \\ C_{61} & C_{62} & C_{63} & C_{64} & C_{65} & C_{66} \end{bmatrix} \begin{bmatrix} \varepsilon_1 \\ \varepsilon_2 \\ \varepsilon_3 \\ \gamma_{23} \\ \gamma_{13} \\ \gamma_{12} \end{bmatrix} \tag{3.1}$$

There are several special cases of symmetry that simplifies the stiffness matrix **C**. Orthotropic, transverse isotropic and isotropic are three such cases. In the case of a material or a structure having 3 mutually perpendicular planes of symmetry where the material properties are independent of direction within each plane, the material is called orthotropic. The stiffness matrix **C** in the orthotropic case is reduced to only 9 independent elastic constants, see matrix 3.2. A special class of orthotropic materials, called transverse isotropic are those that have the same properties in one plane and different properties normal to that plane. A transverse isotropic material can be described by 5 independent elastic constants and has a simpler stiffness matrix, see matrix 3.3. The simplest case if Hookes law is in the isotropic case where the stiffness matrix is given by only

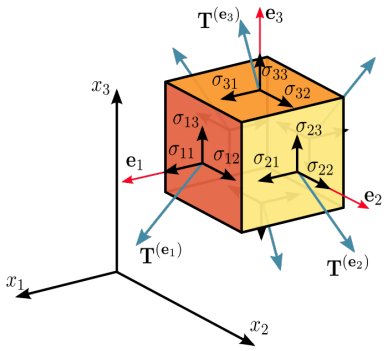

Figure 18: Components of stress in three dimensions.

two elastic constants from equation 3.4.

$$\begin{bmatrix} C_{11} & C_{12} & C_{13} & 0 & 0 & 0 \\ C_{21} & C_{22} & C_{23} & 0 & 0 & 0 \\ C_{31} & C_{32} & C_{33} & 0 & 0 & 0 \\ 0 & 0 & 0 & C_{44} & 0 & 0 \\ 0 & 0 & 0 & 0 & C_{55} & 0 \\ 0 & 0 & 0 & 0 & 0 & C_{66} \end{bmatrix} \tag{3.2}$$

$$\begin{bmatrix} C_{11} & C_{12} & C_{13} & 0 & 0 & 0 \\ C_{12} & C_{11} & C_{13} & 0 & 0 & 0 \\ C_{13} & C_{13} & C_{33} & 0 & 0 & 0 \\ 0 & 0 & 0 & C_{44} & 0 & 0 \\ 0 & 0 & 0 & 0 & C_{44} & 0 \\ 0 & 0 & 0 & 0 & 0 & (C_{11} - C_{12})/2 \end{bmatrix} \tag{3.3}$$

$$\begin{bmatrix} C_{11} & C_{12} & C_{12} & 0 & 0 & 0 \\ C_{12} & C_{11} & C_{12} & 0 & 0 & 0 \\ C_{12} & C_{12} & C_{11} & 0 & 0 & 0 \\ 0 & 0 & 0 & (C_{11} - C_{12})/2 & 0 & 0 \\ 0 & 0 & 0 & 0 & (C_{11} - C_{12})/2 & 0 \\ 0 & 0 & 0 & 0 & 0 & (C_{11} - C_{12}/2 \end{bmatrix} \tag{3.4}$$

3.1.2 Plate theory

The theory presented here follows the text book from C. T. Herakovich [13] on **laminat theory** which is based on plate theory. The reason for specifying laminate theory is due to the possibility to make flexure patterns out of material made up by layers with differnet fiber oriantations, e.g. plywood.

Plate theory is used on flat structural elements with a small thickness compared to the surface dimensions. It uses two-dimensional plane stress theory and is built on the following of Kirchhoffs' assumptions: (1) the mid plane of the plate is the *neutral plane* and is considered stress free, (2) Elements lying perpendicular to the mid plane, also called line elements, remain normal to the mid plane, (3) out of plane strain is neglected. This leads to a simplified stress analysis where σ_3, τ_{23} and τ_{13} is zero.

In plane normal forces, shear force and bending moments and twist moment are given per unit width and is written as.

$$N_x, N_y, N_{xy}, M_x, M_y, M_{xy} \tag{3.5}$$

Curvature κ is the inverse of the curve radius and deflection is w. The curve for small slopes are given as

$$\kappa_x = \frac{1}{R_x} = -\frac{\partial^2 w}{\partial x^2}, \quad \kappa_y = \frac{1}{R_y} = -\frac{\partial^2 w}{\partial y^2}, \quad \kappa_{xy} = \frac{1}{T_{xy}} = -\frac{\partial^2 w}{\partial x \partial y} \tag{3.6}$$

The matrix $\mathbf{Q}$ represents the stiffness matrix for each ply in a laminate, after being subjected to the respective transformations.

$$\begin{bmatrix} \sigma_1 \\ \sigma_2 \\ \tau_{12} \end{bmatrix} = \begin{bmatrix} Q_{11} & Q_{12} & 0 \\ Q_{12} & Q_{22} & 0 \\ 0 & 0 & Q_{66} \end{bmatrix} \begin{bmatrix} \varepsilon_1 \\ \varepsilon_2 \\ \gamma_{12} \end{bmatrix} \tag{3.7}$$

The strains can be coupled into mid-plane strains and strains as a function of the plane curvature.

$$\begin{bmatrix} \varepsilon_x \\ \varepsilon_y \\ \gamma_{xy} \end{bmatrix} = \begin{bmatrix} \varepsilon_x^0 \\ \varepsilon_y^0 \\ \gamma_{xy}^0 \end{bmatrix} + z \begin{bmatrix} \kappa_x \\ \kappa_y \\ \kappa_{xy} \end{bmatrix} \tag{3.8}$$

A laminate has the load-deformation relation where the loads are the same as in plate theory, given per length unit.

$$\begin{bmatrix} N_x \\ N_y \\ N_{xy} \\ M_x \\ M_y \\ M_{xy} \end{bmatrix} = \begin{bmatrix} A_{xx} & A_{xy} & A_{xs} & B_{xx} & B_{xy} & B_{xs} \\ A_{xy} & A_{yy} & A_{ys} & B_{xy} & B_{yy} & B_{ys} \\ A_{xs} & A_{ys} & A_{ss} & B_{xs} & B_{ys} & B_{ss} \\ B_{xx} & B_{xy} & B_{xs} & D_{xx} & D_{xy} & D_{xs} \\ B_{xy} & B_{yy} & B_{ys} & D_{xy} & D_{yy} & D_{ys} \\ B_{xs} & B_{ys} & B_{ss} & D_{xs} & D_{ys} & D_{ss} \end{bmatrix} \begin{bmatrix} \varepsilon_x^0 \\ \varepsilon_y^0 \\ \gamma_{xy}^0 \\ \kappa_x \\ \kappa_y \\ \kappa_{xy} \end{bmatrix} \tag{3.9}$$

For a balanced and symmetric laminate matrix $\mathbf{B} = 0$ and the following matrices are valid. This is the case when an orthotropic unit is considered and everything is symmetric about the mid-plane.

$$\begin{bmatrix} A_{xx} & A_{xy} & 0 \\ A_{xy} & A_{yy} & 0 \\ 0 & 0 & A_{ss} \end{bmatrix}, \begin{bmatrix} D_{xx} & D_{xy} & 0 \\ D_{xy} & D_{yy} & 0 \\ 0 & 0 & D_{ss} \end{bmatrix} \tag{3.10}$$

3.1.3 Material behaviour

The material used in this thesis is *medium-density fiberboard* (MDF). It's properties are not ideal, and in practice, a lot of other materials could be used. There are, however, good reasons for choosing MDF:

- It is cheep
- It is easy accessible
- It can easily be cut with a laser cutter
- It is already a widely used material in living hinge and flexure applications

For the materials used to make flaxure patterns, important characteristics to consider is: linear elasticity, yielding, plasticity, creep, relaxation and thermal expansion.

Elasticity is the property for materials to be deformed non-permanently. In practice materials behave only linearly elastic up to small deformations.

A material or structure can have anisotropic behaviour, which is different properties in different directions. It is important to keep in mind that anisotropic materials in one length scale may be isotropic in another, usually larger, scale. A good example of this are poly-crystalline metals with small grain size. Each grain may be anisotropic, but if the whole material consists of random oriented grains, the measured mechanical properties will, on a larger scale, be measured as the average of the properties over all possible orientation of the individual grain.

Relaxation is a property related to semi-crystalline materials with visco-elastic behaviour. It is observed as decreased stress in response to constant strain in the structure, in a non-linear way. The non-linearity of the response is described by both relaxation and creep. Creep is the the tendency of a solid material to move slowly or deform permanently under the influence of constant mechanical stress. These effects may become

prominent in the materials: MDF, acryllics, epoxy and polystyrene due to their semi-crystalline structure.

Composite materials are made from two or more constituent materials with significant different physical or chemical properties. The mechanical properties of such composites depend on the properties of the constituents and the orientation of the fibers.

3.2 Non-linear effects

As the name indicates, non-linear problems are not linear, and its behaviour could come from a wide range of phenomena, possibly interacting with one another, and each perhaps difficult to formulate. In a lot of practical cases, a linear model provide satisfactory models for simulating a problem, but it is not uncommon to experience non-linearities. [14] An problem becomes non-linear when the e.g. stiffness becomes a function of displacement or deformation. A classical example of a non-linear behaviour is when a deformation caused by a certain load is not doubled when the load is doubled. The relation is not linear and the response of the object subjected to the specific load becomes hard to predict. As Cook phrases it: Non-linear analyses are undertaken more and more often because software become more capable and more widely available, computational costs have declined, more demand are placed upon structures, and more understanding of manufacturing processes is required.[14] The literature explains that there are some main *sources* from where the non-linearities erupts. These are categorized differently between authors, but in structural mechanics the types are: *Material non-linearities; Contact non-linearities; Geometric non-linearities*

From the book used in the course ASEN 6107 at the University of Colorado [15], Felippa Carlos describes these three sources in the following way:

3.2.1 Material non-linearities

Material behaviour depends on current deformation state and possibly past history of the deformation. Other constitutive variables such asprestress, temperature, time, moisture, electro-magnetic fields, etc., may be involved. The engineering significance of material non-linearities varies greatly across diciplines. ... In mechanical engineering creep and plasticity are most important, frequently occurring in combination with strain-rate and thermal effects. Material non-linearities may give raise to very complex phenomena such as *path dependent hysterisis, localization, shakedown, fatigue, progressive failure*.

3.2.2 Geometric non-linearities

This source is apparent when the change in geometry as the structure deforms is taken into account in setting up the strain-displacement and equilibrium equations. It models a myriad of physical problems: *Large strain*: The strains themselves may be large, say over 5%. Examples: rubber structures, metal forming. These are frequently associated with material non-linearities; *Small strains but finite displacement and/or rotations*: Slender structures undergoing finite displacements and rotations although the deformational strain may be treated as infinitesimal. Example: cables, springs, arches, bars, thin plates; *Linearized prebuckling*: When both strains and displacements may be treated as infinitesimal before loss of stability by buckling. These may be viewed as initially stressed members. Example: many civil engineering structures such as buildnings and stiff (non-suspended) bridges.

3.2.3 Contact

In his book Carlos places this source under the category Displacement boundary condition(BC) Non-linearities. In contact, displacement boundary conditions depend on the deformation of the structure. Here *no-interpenetration* conditions are enforced on flexible bodies while the extent of the contact area is unknown. The no-interpenetration conditions is based on checking if nodes on different surfaces are penetrating each others surfaces. The conditions are enforced by constraints often called multifreedom constraints(MFCs), and three common methods for creating them are the *Master-Slave Elimination*, *Penalty Augmentation* and *Lagrange Multiplier Adjunction*.

The contact phenomena is a large subject, and many text books have dedicated several chapters to present modeling techniques, calculation procedures and the different types of contact.

3.3 Critical points

This section presents a key aspect in geometrical non-linear analysis. The study of critical points helps to understand how non-linear behaviour appear physically.

The theory is taken form the curriculum of the course TMM4250 - Advanced Product Simulation, which uses the material from ASEN 6107, a subject at Department of Aerospace Engineering Sciences University of Colorado at Boulder.

3.3.1 Limit points and Bifurcation points

The following statement is given in [15]:

> Along a static equilibrium path of a conservative system, transition from stability to instability can only occur at critical points.

Critical points are classified into *limit points* and *bifurcation points*. Felippa describes the Limit points at which the tangent of the equilibrium path is unique but normal to the λ axis, corresponding to a maximum, minimum or inflexion point with respect to λ. When the limit point is a maximum or a minimum the point is called *snap through* or *snap buckling*. The bifurcation points is described as where two equilibrium path branches intersects, causing there to be no unique tangent. The physical characteristics of a bifurcation point is *an abrupt transition from one deformation mode to another mode*[15]. In figure 19a and 19b two possible orientations of limit points and bifurcation points are shown.

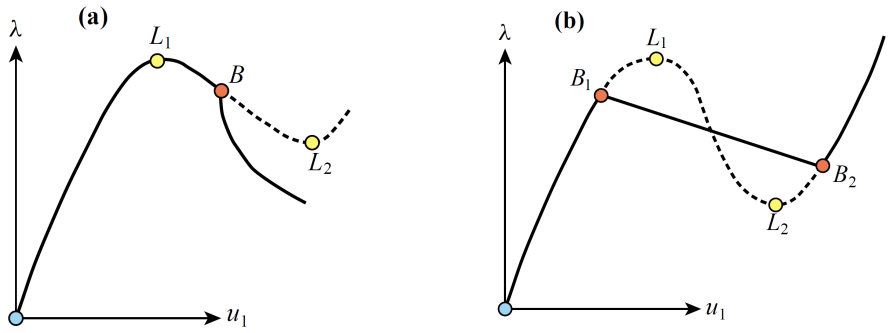

(a) Limit point (*snap through* behavior) L_1 occurs before bifurcation B_1

(b) Bifurcation point B_1 occurs before limit point L_1, in which case L_1 is physically unreachable

Figure 19: Critical points for a two degree of freedom system (u_1, u_2) shown on the u_1 versus λ plane. Full lines represent physically preferred paths.

4 Numerical modelling and analysis

4.1 Objectives

There are hundreds of possible flexure patterns, each with the equal amount of different applications. A systematic study and characterization has not yet been done, and would require a great amount of time. For that reason, the current work only covers fundamental cases typically encountered when dealing with flexure patterns.

Additionally, the study has been chosen to address a designers point of view and usage, due to the applications the flexure patterns have in the makerspace community. Web forums such as Pinterest, Instructables and similar, spread and develop the patterns at a great pace, and the people there represent the major bulk of the user group. With this in mind the following choices were made:

4.1.1 The patterns

In the project work [5] multiple patterns were explored, but the most used was the pattern consisting of the LET flexure from section 2.2, seen in figure 20a. Made by introducing simple cuts, it is often just called the *slits* pattern.

The second most used pattern, a bit more complicated, was the one called *YdX*, see figure 20b. The name comes from the association to the letters Y and X, and is pronounced *wide-ex*.

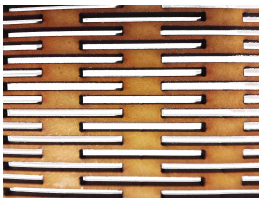

(a) A LET pattern made onto MDF

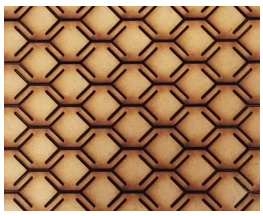

(b) The YdX pattern made onto MDF

Figure 20: The two patterns studied in this work

This thesis continues the study of these patterns for several reasons:

One of the features of the slits is to be elastic and rigid in perpendicular directions, respectively. It is intuitive in design, has a lot of applications, and is frequently used in different maker space communities - a quick web search on *living hinges* verifies that. Consequently, main reasons for the choice was that it is widespread and has applications easy to relate to.

The YdX was chosen as a counterpart to the simple slits pattern, as it is more uncommon, interesting in design and show to have an auxetic behaviour, introduced in section 2.3. It's deformations are a lot more complicated due to having cuts/edges that are not perpendicular or parallel to the load axes. This is discussed in more detail in section 4.2.3.

Each of the patterns are made from a repeating unit subjected to a specific repeating pattern. Both the slits and the YdX pattern are made from the units seen in figure 21a

and 21b, respectively.

(a) Slit repeating unit

(b) YdX repeating unit

Figure 21: The two repeating units

4.1.2 Transition criteria

When performing a non-linear study, an interesting part to look into is the transition area from the linear regime to the non-linear. This transition could have significance for calculations or analytic studies based on the linear models, where non-linear sources would render the results doubtful. To find this transition, a threshold value is needed. When comparing the data from a linear and a non-linear analysis of a given model, this threshold will give a criteria on how far they can deviate from one another before the analysis gives two different results.

This section discusses how this threshold value is chosen. Let it be noted that the criteria is not based specifically on safety, as would be natural for many other engineering applications, but instead on a designers preferences. However, the safety factor could play a part in this choice in the future.

For design purposes, the flexibility or the ability to flex in different directions while maintaining a degree of stiffness from the base material, is one of the most attractive reasons for using a flexure pattern. The question is, however, which is most important for a designer; higher compliance or higher stiffness? For example, when a designer wants to make a new lamp shade from a flat piece of MDF, a high compliance would make it easier to accomplish the cylinder form seen in figure 22. This could, however, result in a too soft construction. The alternative would be a too stiff construction, making it harder to join the two ends together. For a designer the first alternative would seem favorable, considering the visual effect and the proof of concept. Consequently, the designer making the lamp shade could compensate for a non-linear stiffening by choosing a softer pattern to begin with.

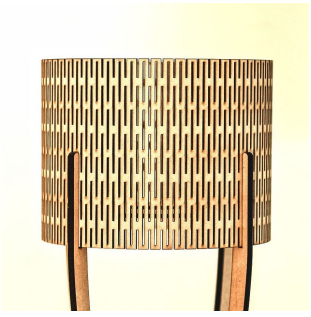

Figure 22: A lamp screen made out of MDF with an integrated LET pattern. Picture: [3]

Viewed from the opposite direction, there is the situation where the designer makes

a similar lamp shade and have to choose the *pattern parameters* to acquire the correct stiffness. Not considering the non-linear effects could result in a stiffness deviation from the calculated load, varying with the magnitude of the deformation. If, however, the designer knew that there would be a 10% deviation for a given deflection or load, he could compensate for it.

Based on this reasoning, the analyses will set out to find the suggested 10% deviation from for both patterns and for different parameters. There are multiple ways of measuring the deviation from the linear curve.

- 10% strain offset
- 10% load offset
- 10% secant slope offset
- 10% secant angle offset

For simplicity and readability in a graph, the load offset was chosen.

4.2 Modelling

4.2.1 Approach

The analyses were performed by the help of computer simulations. In this study a conventional code in the software ABAQUS has been used. It offers a well established modelling environment compatible with the coding language Python to create and submit jobs. It is based on the *Finite Element Method*, which is a widely used numerical method for solving engineering problems. The finite element system ABAQUS/STANDARD has been chosen for its general-purpose applicability. It uses a traditional implicit solution technique, suited for static, low-speed dynamic, or steady-state transport analyses [4].

The main motivation for using numerical calculations software in this study is the ability to explore all kinds of patterns, and be able to perform test in an ideal environment.

For the current work static stress analyses is used, which could be both linear or non-linear. This choice is easily made by switching the large-displacement formulation *Nlgeom* in the steps *ON* or *OFF*. Nlgeom stands for *non-linear geometric behaviour*.

With ABAQUS, scripting in python was used. The codes written for the analyses in this thesis is given in the appendix in part D B.

4.2.2 Repeating unit

The base models of the repeating units found in the two patterns introduced in section 4.1.1, in figure 20a, was made in ABAQUS, see figure 23a and 23c. The python script producing the parts fetched model parameters from a text file. How these parameters were defined are shown in figure 23b and 23d. Using python with ABAQUS made it easier to generate sketches for different dimensions, which again enabled a parameter study of the patterns.

The model parameters for the slits and YdX are given in table 7a and 7b, respectively. The different colors highlights the variation of the main model parameters.

ModelName	eSize	eMod	pois	a	b	c	d	thickness
m001	1	3689	0.24	10	50	7	1.5	1.5
m002	1	3689	0.24	10	60	7	1.5	1.5
m003	1	3689	0.24	10	70	7	1.5	1.5
m004	1	3689	0.24	10	80	7	1.5	1.5
m005	1	3689	0.24	10	90	7	1.5	1.5
m006	1	3689	0.24	10	100	7	1.5	1.5
m007	1	3689	0.24	10	50	7	1.5	1.5
m008	1	3689	0.24	10	50	7	1.4	1.5
m009	1	3689	0.24	10	50	7	1.3	1.5
m010	1	3689	0.24	10	50	7	1.2	1.5
m011	1	3689	0.24	10	50	7	1.1	1.5
m012	1	3689	0.24	10	50	7	1	1.5
m013	1	3689	0.24	10	50	7	1.5	1.5
m014	1	3689	0.24	10	50	6	1.5	1.5
m015	1	3689	0.24	10	50	5	1.5	1.5
m016	1	3689	0.24	10	50	4	1.5	1.5
m017	1	3689	0.24	10	50	3	1.5	1.5
m018	1	3689	0.24	10	50	2	1.5	1.5
m019	1	3689	0.24	10	50	7	1.5	1.5
m020	1	3689	0.24	9	50	7	1.5	1.5
m021	1	3689	0.24	8	50	7	1.5	1.5
m022	1	3689	0.24	7	50	7	1.5	1.5
m023	1	3689	0.24	6	50	7	1.5	1.5
m024	1	3689	0.24	5	50	7	1.5	1.5

(a) Parameters used for the LET geometric non-linear analysis

ModelName	eSize	eMod	pois	a	b	c	d	theta	thickness
m001	1	3687	0.24	4.5	9	2.5	0.85	45	1.5
m002	1	3687	0.24	4.5	10	2.5	0.85	45	1.5
m003	1	3687	0.24	4.5	11	2.5	0.85	45	1.5
m004	1	3687	0.24	4.5	12	2.5	0.85	45	1.5
m005	1	3687	0.24	4.5	13	2.5	0.85	45	1.5
m006	1	3687	0.24	4.5	14	2.5	0.85	45	1.5
m007	1	3687	0.24	4.5	9	2.5	0.85	45	1.5
m008	1	3687	0.24	4.5	9	2.5	0.95	45	1.5
m009	1	3687	0.24	4.5	9	2.5	1.05	45	1.5
m010	1	3687	0.24	4.5	9	2.5	1.15	45	1.5
m011	1	3687	0.24	4.5	9	2.5	1.25	45	1.5
m012	1	3687	0.24	4.5	9	2.5	1.35	45	1.5
m013	1	3687	0.24	4.5	9	2.5	0.85	45	1.5
m014	1	3687	0.24	4.5	9	2.4	0.85	45	1.5
m015	1	3687	0.24	4.5	9	2.3	0.85	45	1.5
m016	1	3687	0.24	4.5	9	2.2	0.85	45	1.5
m017	1	3687	0.24	4.5	9	2.1	0.85	45	1.5
m018	1	3687	0.24	4.5	9	2	0.85	45	1.5
m019	1	3687	0.24	4.5	9	2.5	0.85	45	1.5
m020	1	3687	0.24	5	9	2.5	0.85	45	1.5
m021	1	3687	0.24	5.5	9	2.5	0.85	45	1.5
m022	1	3687	0.24	6	9	2.5	0.85	45	1.5
m023	1	3687	0.24	6.5	9	2.5	0.85	45	1.5
m024	1	3687	0.24	7	9	2.5	0.85	45	1.5

(b) Parameters used for the YdX geometric non-linear analysis

Table 7: The model parameters

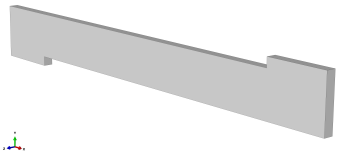

(a) The base model made in ABAQUS

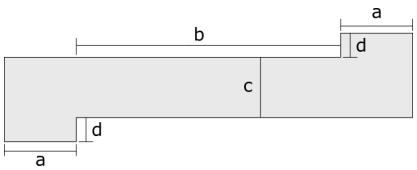

(b) The varying model parameters used to produce the slits

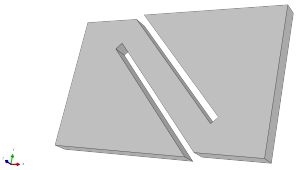

(c) The base model made in ABAQUS

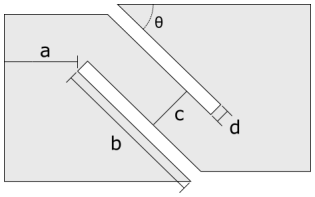

(d) The varying model parameters used to produce the YdX

Figure 23: The base models in ABAQUS and its parameters

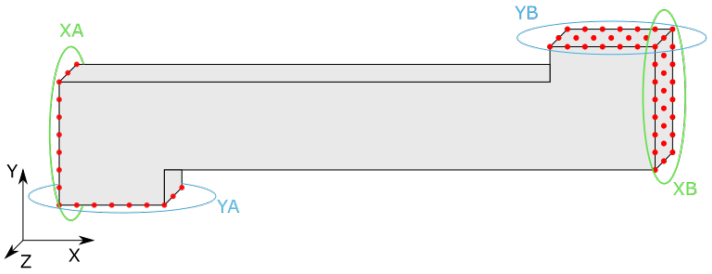

Figure 24: Labeling of the model sides

The values for the parameter study was chosen based on a tactile study in the project work. Having the model sized in this manner, creates a pattern that has good flexibility, but is not too small that it breaks easily when flexed. The interval between each parameter value was also chosen based on previous experience with the patter.

The script produced the base part in the positive octant of the coordinate system. The model was then mirrored about the XY-plane. For this operation, an orphan mesh was made because there are no guaranties to get coincident nodes on the mirror surface if the part is mirrored first, merged with the new part and *then* meshed. Creating an mesh part from the model before mirroring would solve this problem. In addition, an orphan mesh provides the opportunity to control the deformations of each specific node on the model surfaces. This enables the implementations of the needed boundary conditions introduced in section 8. A solid part consists of only corner nodes and surfaces in between. Thus, the alternative would be to partition the part enough times to get the required nodes.

4.2.3 Loads and Boundary Conditions

In addition to having two different patterns, it is important to clearly distinguish the analyses based on the different loads and boundary conditions. The two load cases are *in-plane tension* and *cylindrical bending*, which has physical properties described with the plate theory from section 3.1. Shown as equations, ther are, respectively:

In-plane tension

$$\begin{bmatrix} N_x \\ N_y \\ N_xy \end{bmatrix} = \begin{bmatrix} A_{xx} & A_{xy} & 0 \\ A_{xy} & A_{yy} & 0 \\ 0 & 0 & A_{ss} \end{bmatrix} \begin{bmatrix} \varepsilon_x \\ \varepsilon_y \\ \gamma_{xy} \end{bmatrix} \tag{4.1}$$

and

$$\begin{bmatrix} M_x \\ M_y \\ M_{xy} \end{bmatrix} = \begin{bmatrix} D_{xx} & D_{xy} & 0 \\ D_{xy} & D_{yy} & 0 \\ 0 & 0 & D_{ss} \end{bmatrix} \begin{bmatrix} \kappa_x \\ \kappa_y \\ \kappa_{xy} \end{bmatrix} \tag{4.2}$$

.

Figure 24 shows how the boundaries on the model are named. The YdX model is labeled in the same way.

The boundary conditions at XA and YA are apparent in every analysis and constrains the model from translating in X and Y directions, respectively. In addition, the midplane node at $(x = 0, y = 0)$, are constrained in Z. The BC at the other controls XB to be either constrained or unconstrained in X. These two cases causes the equations 4.1 and 4.2 to

Geometric non-linear analysis of Slits			
In-plane tension		Cylindrical bending	
$N_x \neq 0, N_y \neq 0, \varepsilon_y \neq 0$	$N_y \neq 0, \varepsilon_x \neq 0, \varepsilon_y \neq 0$	$M_x \neq 0, M_y \neq 0$	$M_x \neq 0, M_y \neq 0$

Geometric non-linear analysis of YdX			
In-plane tension		Cylindrical bending	
$N_x \neq 0, N_y \neq 0, \varepsilon_y \neq 0$	$N_y \neq 0, \varepsilon_x \neq 0, \varepsilon_y \neq 0$	$M_x \neq 0, M_y \neq 0$	$M_x \neq 0, M_y \neq 0$

Contact non-linear analysis of Slits
Cylindrical bending
$M_x \neq 0, M_y \neq 0$

Contact non-linear analysis of YdX
Cylindrical bending
$M_x \neq 0, M_y \neq 0$

Table 8: Overview of the different load cases

become:

Constrained

$$\begin{bmatrix} N_x \\ N_y \\ 0 \end{bmatrix} = \begin{bmatrix} A_{xx} & A_{xy} & 0 \\ A_{xy} & A_{yy} & 0 \\ 0 & 0 & 0 \end{bmatrix} \begin{bmatrix} 0 \\ \varepsilon_y \\ 0 \end{bmatrix} \tag{4.3}$$

$$\begin{bmatrix} M_x \\ M_y \\ 0 \end{bmatrix} = \begin{bmatrix} D_{xx} & D_{xy} & 0 \\ D_{xy} & D_{yy} & 0 \\ 0 & 0 & D_{ss} \end{bmatrix} \begin{bmatrix} 0 \\ \kappa_y \\ 0 \end{bmatrix} \tag{4.4}$$

Unconstrained

$$\begin{bmatrix} 0 \\ N_y \\ 0 \end{bmatrix} = \begin{bmatrix} A_{xx} & A_{xy} & 0 \\ A_{xy} & A_{yy} & 0 \\ 0 & 0 & A_{ss} \end{bmatrix} \begin{bmatrix} \varepsilon_x \\ \varepsilon_y \\ 0 \end{bmatrix} \tag{4.5}$$

In cylindrical bending the BC at XB was not set to unconstrained because the moment has little relevance for the strain in x. The constraints in XB simulates two different boundary conditions often encountered in flexure patterns. The two cases are shown in figure 25a, where unit cell *A* is the constrained case and *B* the unconstrained one. This can be compared to the scenario seen in figure 25b.

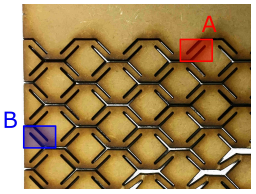

(a) The two different cases for constraining the sides of the unit cell

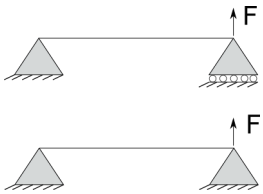

(b) The equivalent constraining model

Figure 25: The different boundary conditions

Table 8 lists all the cases run in this study.

(a) Bending in the LET flexure of the slits (b) Torsion in the LET flexure of the slits

Figure 26: Deformations in the flexure of the slits

The second boundary condition on the XB side is apparent in every analysis. This BC controls how the nodes deflect relative to one another causing the side surface to remain plane and vertical for any load case. In this manner, the edge continuity is satisfied.

4.2.4 Geometric Non-Linearity

In the scope of this particular study, only two load cases were used: in-plane tension and cylindrical bending, along the y-axis. These are the two most fundamental deformations a flexure pattern is subjected to. The plain tension had a its strain set to the unit size of one, for the purpose of having a large deformation easily followed in increments of 0.1. In cylindrical bending, curvature was the most practical variable to use. Its value was set to 0.05 which corresponds to a curvature radius of 20 mm. This is not an uncommon value for bending of different patterns. Subjecting the patterns to large deformations introduces geometric non-linearities. Commonly, strain at about 0.5% and above are counted as large. For flexure patterns, and especially the LET pattern, a magnitude of 0.05 strain is not uncommon. This has to do with the LET flexures ability to deform. In-plane tension in Y causes the flexure to be bent as a constrained beam, while cylindrical bending in Y gives a torsional moment in the flexure. These two deformations are shown in figures 26a and 26b. The torsion of the flexure introduces a shear component that would not be apparent in the first case.

The implementation of in-plane tension was straight forward: The nodes on the YB surface was given a deformation in Y for each static step in the simulation.

Load case number two was made to induce a pure moment about Y with the chosen curvature. To manage this, some equations had to be established. More details on the implementation of the moment are found in the contact analysis, section 4.2.5, due to its significance there.

In addition to the load cases, the number of sub-steps in the analysis was chosen. The value would control how fine the resolution of the results would become, seen that each step had about 10 increments. Additionally, in an implicit solver as ABAQUS/STANDARD, the most reliable result is in the last increment of each step, giving a good reason for having more than only one step. After some experimentation the number of sub-steps was chosen to be 10.

4.2.5 Contact

From section 3.2 non-linearities associated with contact is often complex. Initially in ABAQUS, when two solids meet, they do not interact with each other - that is, they are able to move freely into each other. Hence, to simulate a contact, an interaction with by a contact pair had to be made. In ABAQUS this is done by choosing two surfaces and defining one of them as the master surface, and the other as a slave surface. As a result of

the part being a mesh part, acquiring the wanted surfaces by python commands turned out to be involving. The reason was that a mesh do not have any surface object to select, as one would select a node or an element. The solution to this surface selection problem was this:

- Select all the elements having a face at the wanted surface area
- Select all the nodes lying in the wanted surface area
- Loop through the first listed node in all the selected element objects and check if its label/number identification is the same as one of the nodes at the surface area
- If it does: Check to see if the second listed node in the element object is one of the surface node
- And so on...

By doing this, the correct faces lying on the surface of all the relevant elements could be found, and selected into the surface constructor function.

The contact problem for this analysis was chosen based on previous experience with the LET hinge: when bending a sheet with this pattern, the torsion of the beam flexures cause the slits to close on one side, see figure 27. In this closing contact is significant, and removes some of the patterns compliance. The base repeating unit of the slits does not have any slits, so the assembly instance had to be modified. The model was extended, mirrored about the xz-plane, see figure 28. The two surfaces chosen as the contact pair was the two long inside surfaces of the created slit, see figure 66 for reference. These surfaces was guessed to be the only interacting ones.

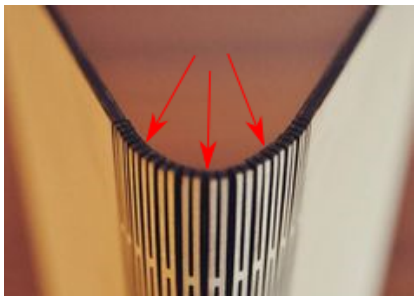

Figure 27: Possible contact points when bending the LET pattern

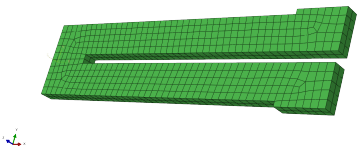

Figure 28: The new assembly model for the bending implementation

The amount of steps in a contact analysis should be chosen to give sufficiently accurate result throughout the whole simulation, and not just the the last increment, which would be the case with only a single step. To see the difference between a single and multiple sub-steps, both cases where run.

Some time was spent on figuring out how to apply a correct deformation to the model.

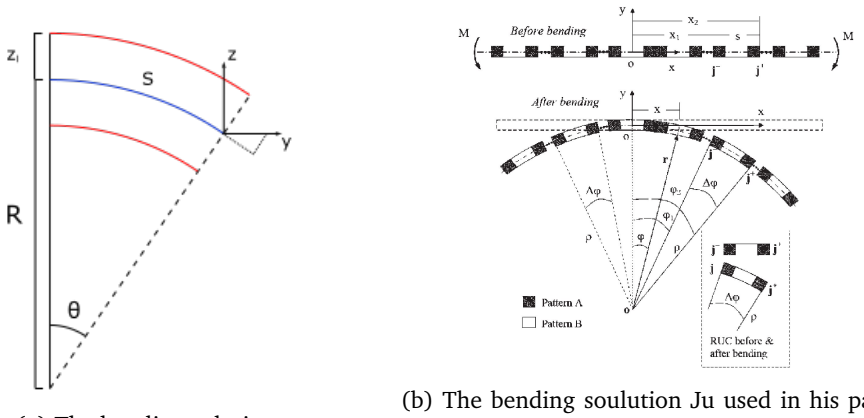

(a) The bending solution

(b) The bending soulution Ju used in his paper, [16]

Figure 29: The bending formulations

The load case wanted was cylindrical bending along y, inducing pure moment M_y. One attempt proved to be useful. It was based on making the boundary condition of the end surfaces YB and YC parallel to the radius line resulting from the curvature. In figure 29a the geometry resulting from these BCs are shown, and the node deformations in y and z-directions, respectively became:

$$\Delta y = \sin\theta(R + z_l) - S \tag{4.6}$$

$$\Delta z = \sin((\pi/2) - \theta)(R + z_l) - (R + z_l) \tag{4.7}$$

Here z_l is the local z-distance from the middle line to the node position, R is the radius of curvature, and θ is the angle between the two end planes of the unit cell.

It was found that Feng Ju et al. [16] had done a similar approach in a situation much like this of the slits. In his paper, he models medical stents as structural beams with a repeating unit cell(RUC) - just like the slits in the current case.

He defines the two outer surface planes of the unit cell which has a periodic boundary condition, as j^- and j^+, see figure 29b. In the stent model, there are two different patterns considered as two different materials. His formulations of the homogeneous displacements after cylindrical bending,

$$\begin{aligned} \bar{u}_x &= -[x - (\rho + y)\sin\phi] \\ \bar{u}_y &= -(\rho + y)(1 - \cos\phi) \end{aligned} \tag{4.8}$$

which is the same as equations 4.6. Note that x and y in 4.8 corresponds to y and z in the slits cross section. Ju points out that for heterogeneous beams with periodic structural patterns the actual displacements are generally not equal to these equations, but rather:

$$\begin{aligned} u_x &= \bar{u}_x + u_x^* = -[x - (\rho + y)\sin\phi] + u_x^* \\ u_y &= \bar{u}_y + u_y^* = -(\rho + y)(1 - \cos\phi) + u_y^* \end{aligned} \tag{4.9}$$

In this equation the term u_x^* and u_y^* has been added. They represents variations from the homogeneous displacements due to material or structural heterogeneity.

Next, Ju defines the periodic boundary conditions on the two end surfaces of the RUC. After converting the equations of 4.9 into cylindrical coordinates, he uses the assumptions that the variations u_r^* at each of the end surfaces are equal, and then cancel each other out in the periodic BC equations - which in catesian coordinates look like:

$$\begin{aligned} u_x|^{j^+} \sin\Delta\phi/2 + u_y|^{j^+} \cos\Delta\phi/2 - u_x|^{j^-} \sin\Delta\phi/2 - u_y|^{j^-} \cos\Delta\phi/2 &= 0 \\ u_x|^{j^+} \cos\delta\rho/2 - u_y|^{j^+} \sin\delta\rho/2 - u_x|^{j^-} \cos\delta\rho/2 - u_y|^{j^-} \sin\delta\rho/2 &= 2y \sin\delta\rho/2 \\ u_z|^{j^+} - u_z|^{j^-} &= 0 \end{aligned} \tag{4.10}$$

In the slits model boundary conditions had not been used, but because the unit cell was symmetrical about the xz-plane, the periodic BCs was achieved by adding the same load on each side of the model.

Following from the laminate theory and Krichoffs' assumptions, the neutral plane or mid plane in a symmetrical sheet should be strain free during cylindrical bending. This was verified by creating a homogeneous model seen in figure 30, and adding the above bending equations. The two figures 30a and 30a shows the strain field of small and large curvature, respectively. During large deformations, observable variations at the edges are seen. They appear because the bending formulations does no give an exact strain through the thickness of the sheet as a result of material properties. For comparison, the same homogeneous model but with Poisson ration of zero was simulated, see figure 31a and 31a. The strain fields of these models are much more consistent and has little edge effects.

(a) Small deformation of a homogeneous model (b) Large deformation of a homogeneous model

Figure 30: Verification of bending functions

(a) Small deformation (b) Large deformation

Figure 31: Homogeneous models with zero Poisson number

4.3 Elements

The mesh properties that needed to be set was the element type and element size. The element type was chosen based on knowledge on the properties of the different alternatives. Because the ABAQUS/Standard was being used, one of the requirements was that the element type should be found in this FE-analyzer. Secondly, an element compatible

with stress/displacement is needed. Based on these two conditions, there are several element families to choose from, but because the model in the current work is a solid part, the obvious choice would be one of the solid elements, shown in figure 32. The solid (or continuum) elements in ABAQUS can be used for linear analysis and for complex nonlinear analyses involving contact, plasticity, and large deformations [4].

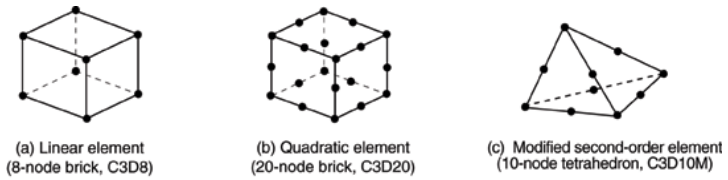

Figure 32: Elements from the family of Solid Elements.(ABAQUS Documentation [4])

Two common and widely used elements i 3D is the first-order 8-node and second-order 20-node brick elements. In ABAQUS it is possible to choose between fully and reduced integration for these element types. The reduced ones uses lower-order integration to find the element stiffness, lowering the time needed for the calculation. From the ABAQUS documentation [4], it is stated that "second-order reduced-integration elements in Abaqus/Standard generally yield more accurate results than the corresponding fully integrated elements. However, for first-order elements the accuracy achieved with full versus reduced integration is largely dependent on the nature of the problem." A challenge with the reduced first-order 8-node brick element is the emergence of hourglass modes, seen in figure 33. Because the model used in this case has possibly very thin sections, this could pose a problem. Although this usually can be avoided by refining the mesh, it would be more convenient to eliminate the risk, due to the mesh in this case is being generated automatically.

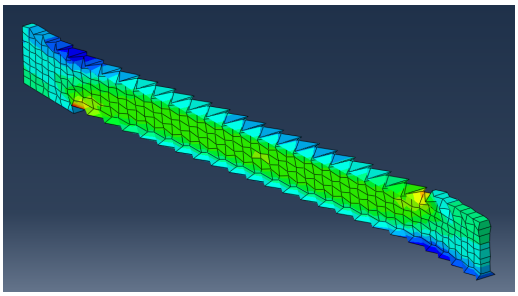

Figure 33: A hourglass mode of the model when using C3D8R elements

The choice between these two element types and the element size was based on a mesh convergence test executed in python. The two element types was compared in two separate load cases - one with a in-plane tension in Y and the other with cylindrical bending in Y.

From the discussion of the convergence test in section 5.1, in addition to the criteria and possible problems noted above, it was concluded that the C3D20R element would be suitable, and a mesh size of about 1 mm would yield accurate results without consuming too much computational time. The element size is inserted into the seeding part of the code, which ABAQUS uses as a reference when seeding the part.

5 Results and Discussion

5.1 Mesh convergence tests

The results in this section where applied in the process of making the base model, used in the other analyses.

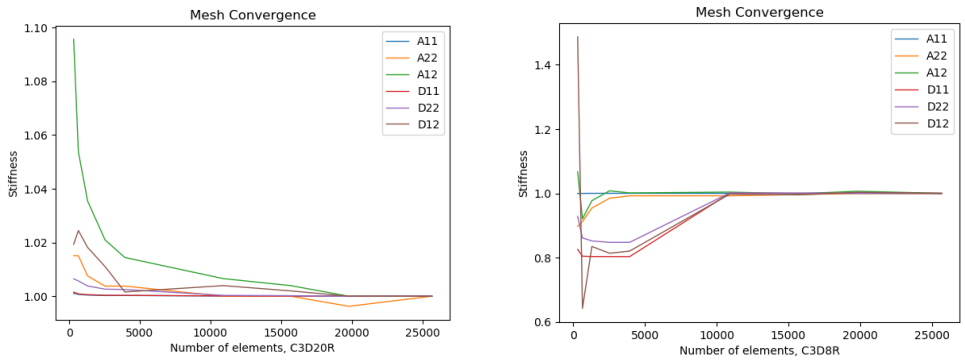

(a) C3D20R

(b) C3D8R

Figure 34: Convergence of the stiffness matrix with respect to the amount of elements

Element Size	Number of elements	Relative CPU time [sek]
5.5	320	3
2.75	656	5
1.833	1312	12
1.375	2544	19
1.1	3944	34
0.916	10912	145
0.785	15696	229
0.687	19792	307
0.611	25680	477

Table 9: Relative CPU time of different C3D20R element sizes

The results here show a clear convergence of the relevant components of the stiffness matrix 3.10. The figures, 34a and 34b, are different due to the properties of the element types. The C3D20R and the C3D8R are a second-order and first-order brick element, respectively. From the graphs is is clear that both types converge towards stable values for the stiffness parameters. The C3D20R has a smaller variation area for coarse elements than the C3D8R, but has a slower convergence rate. At element number of 20000, the A22 has a slight deviation for the second-order element, but it is quite small - the deviation of A12 in C3D8R at the same amount of element, could be of the same magnitude. The variation could come from a sudden change in number of elements in through the beam section.

The most significant aspect is the time used on the simulations. The simulation with the first-order brick elements used a fraction of the time the C3D20R simulations took, at

Element Size	Number of elements	Relative CPU time [sek]
5.5	320	1
2.75	656	1
1.833	1312	2
1.375	2544	3
1.1	3944	6
0.916	10912	18
0.785	15696	30
0.687	19792	39
0.611	25680	54

Table 10: Relative CPU time of different C3D8R element sizes

high number of elements. However, the accuracy of the C3D20R results are a lot better for low element numbers, when the simulation times are more equal. To conclude, due to the higher reliability of the 20-node brick element, this one was used. In addition, a sufficiently small element size was deduced from the result and applied in the following analyses.

5.2 Geometric non-linear analyses

From section 4.1.2, an error or deviation criteria was chosen to serve as a tool when analyzing the results. The value indicated the transition at which the load-deformation curve became non-linear. In the following figures, this transition is marked between two vertical, red lines, giving the strain or curvature area where the value of 10% deviation is reached, for both the LET pattern and the YdX.

Following the linear-non-linear plots for all the load cases, comes the plots that shows how the transition values varies with the different parameter values. These transition plots for the unconstrained cases are also included here.

5.2.1 In-plane tension

Slits:

The following pages contain plots of the results for in-plane tension of the slits.

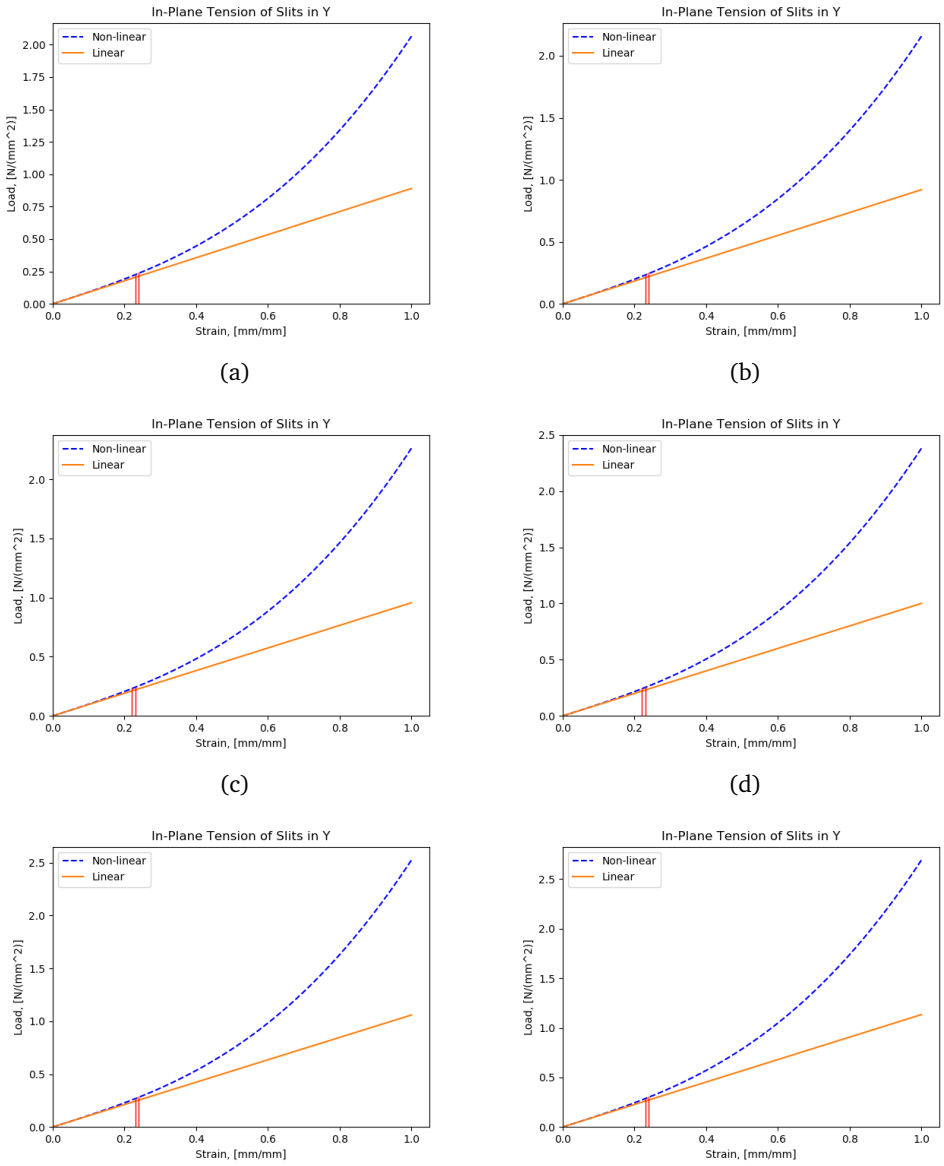

Figure 35: Results from varying parameter a in the Slits

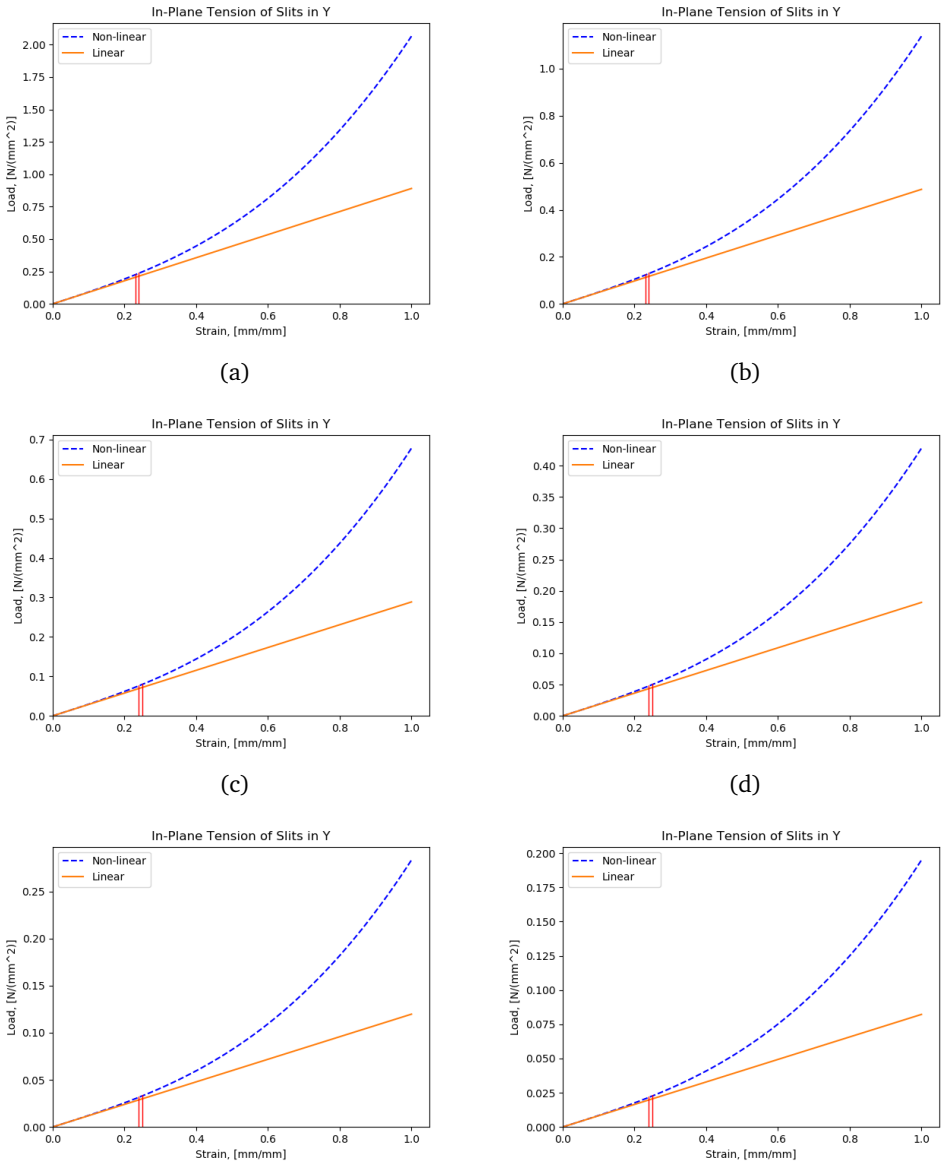

Figure 36: Results from varying parameter b in the Slits

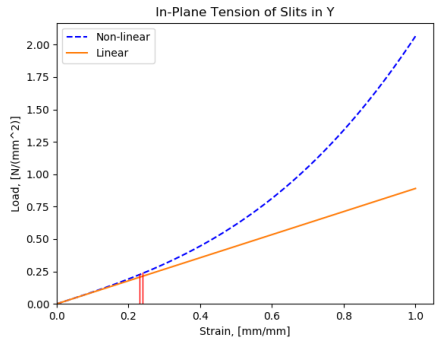

(a)

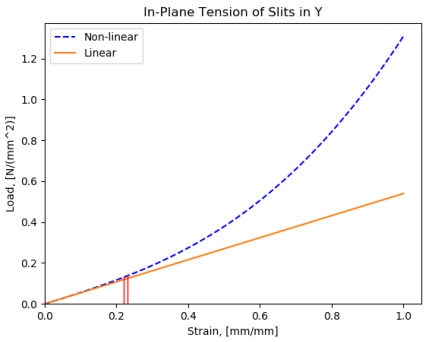

(b)

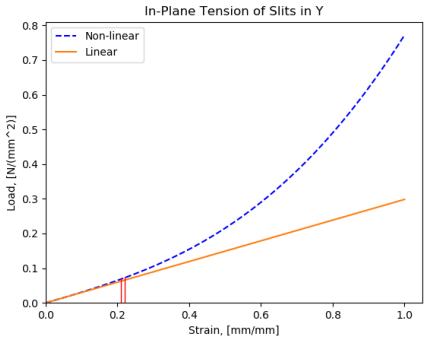

(c)

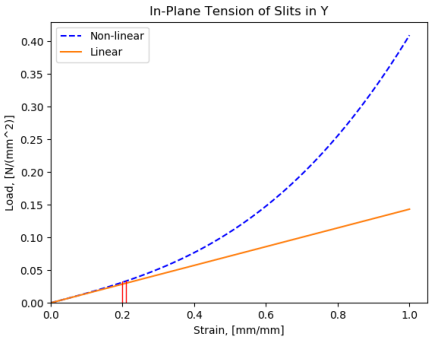

(d)

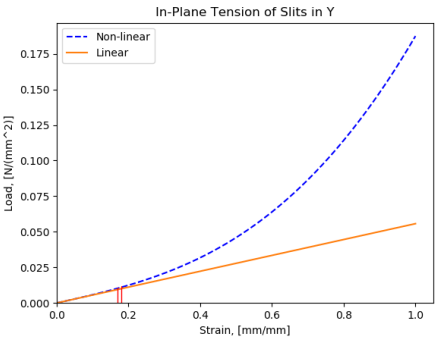

(e)

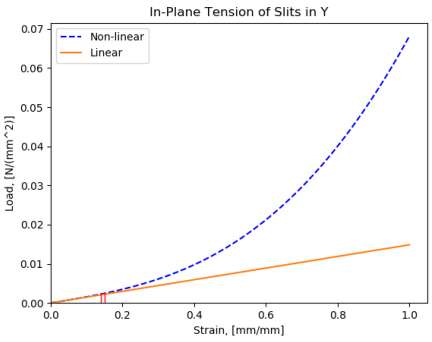

(f)

Figure 37: Results from varying parameter *c* in the Slits

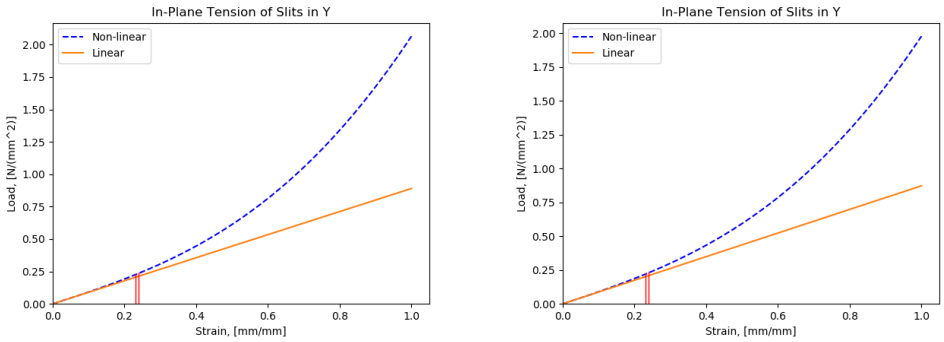

(a)

(b)

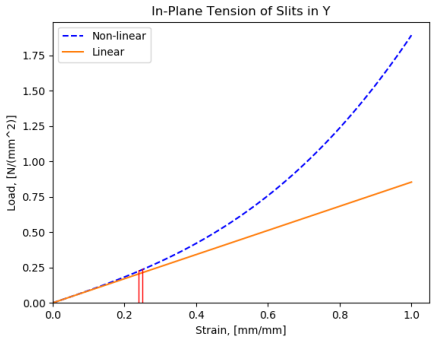

(c)

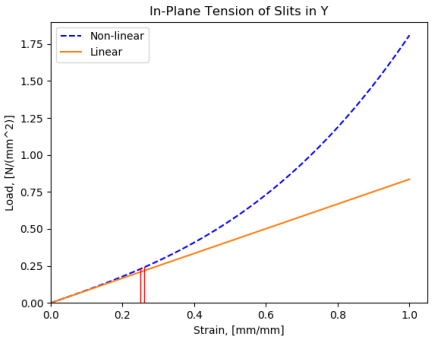

(d)

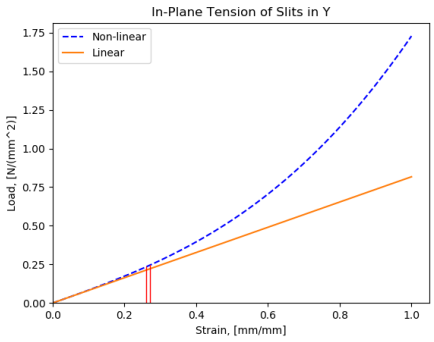

(e)

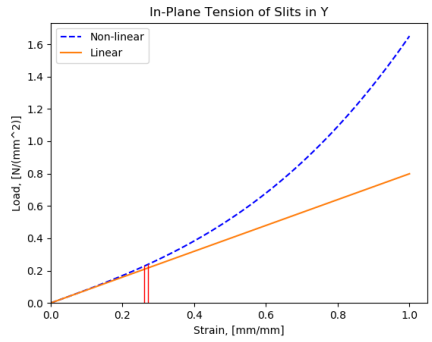

(f)

Figure 38: Results from varying parameter d in the Slits

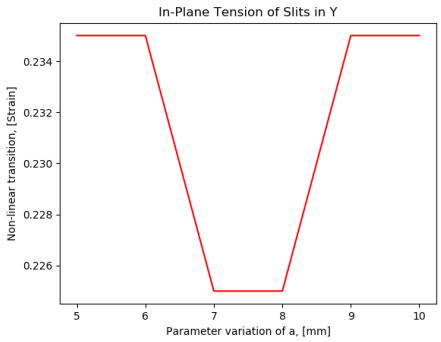

(a)

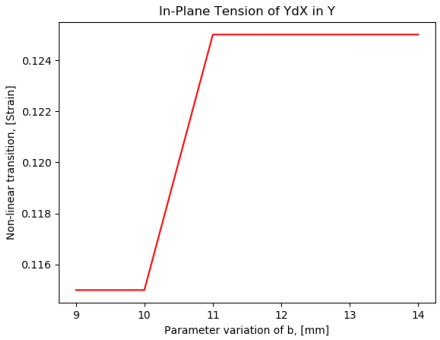

(b)

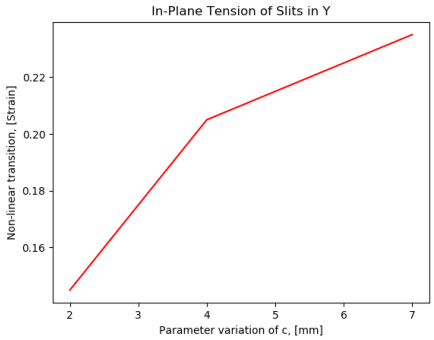

(c)

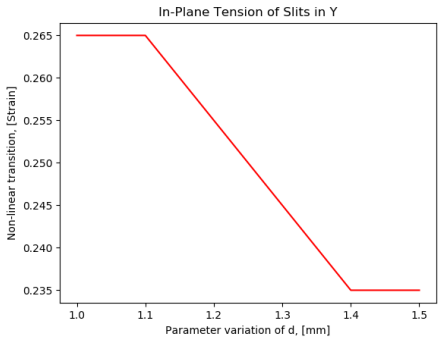

(d)

Figure 39: Plots of the transition values in the Slits for plane tension in Y

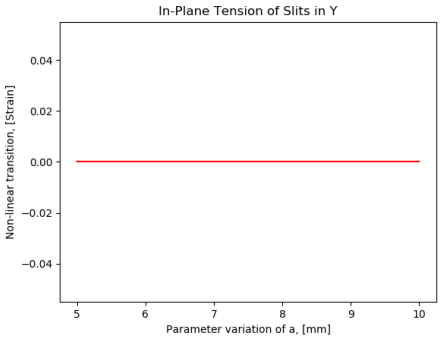

(a)

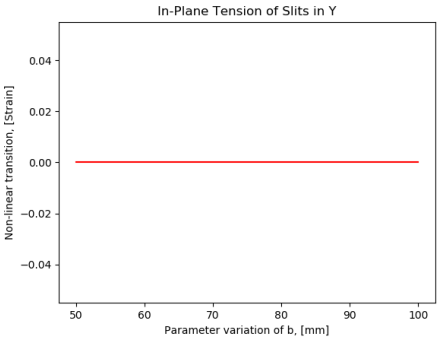

(b)

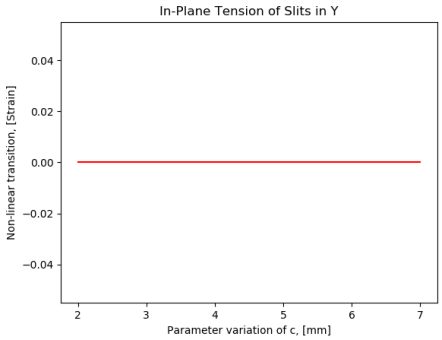

(c)

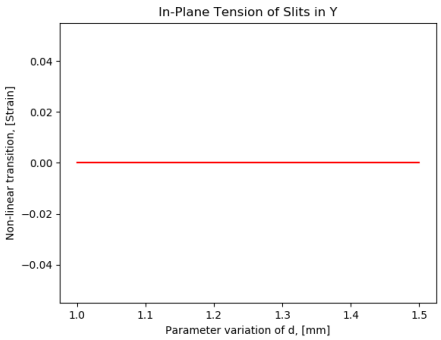

(d)

Figure 40: Plots of the transition values in the Slits for plane tension in Y, unconstrained in XB

Comments on the results

The deformations for slits with in-plane tension are shown in figure 41.

Figure 41: In-plane tension deformation sequence for Slits

What could be said about these result is that none of the parameter variations but parameter *c* causes a significant change in the transition value. When varying the flexure height *c* from 2 to 7 mm the strain transition value moves from about 0.15 to 0.23 which indicates that the slit pattern has a greater resistance to non-linear effects as the flexure beam becomes larger/stiffer. The drop in transition value when varying parameter *a*, could have something to do with a sudden change in element number and distribution. The difference is too small to bo of any significance.

As expected, the unconstrained case causes the geometric non-linearities to be within the significant area of 10% deviation. This means that the boundary conditions, e.g. the position of the repeating unit as in figure 25a, plays an important role when dealing with geometric non-linearities. The zero value in the plots 40, does not mean that the error criteria has been reached at the initial displacement. The value automatically is set to zero when the transition is inside the 10% criteria.

YdX:

The following pages contain plots of the results for in-plane tension of the YdX.

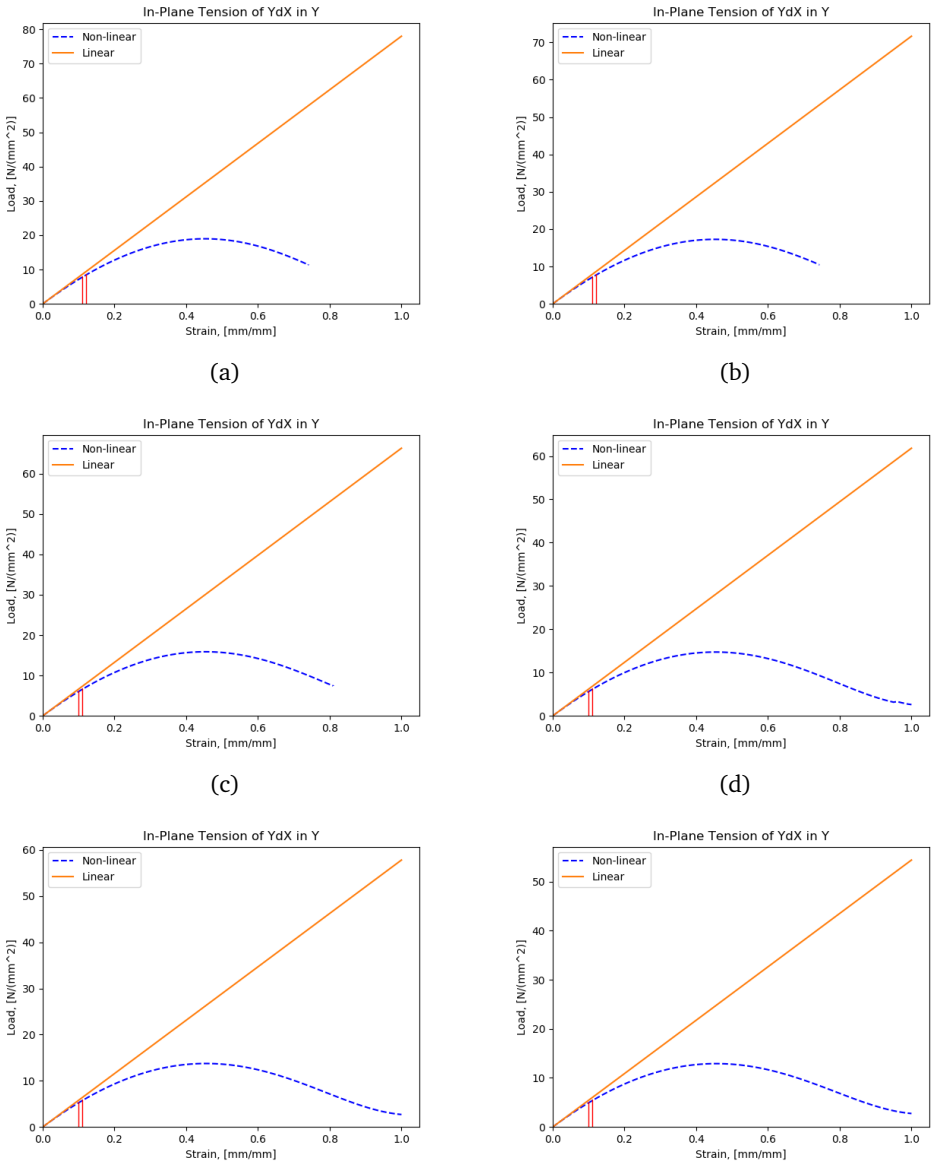

Figure 42: Results from varying parameter a in the YdX

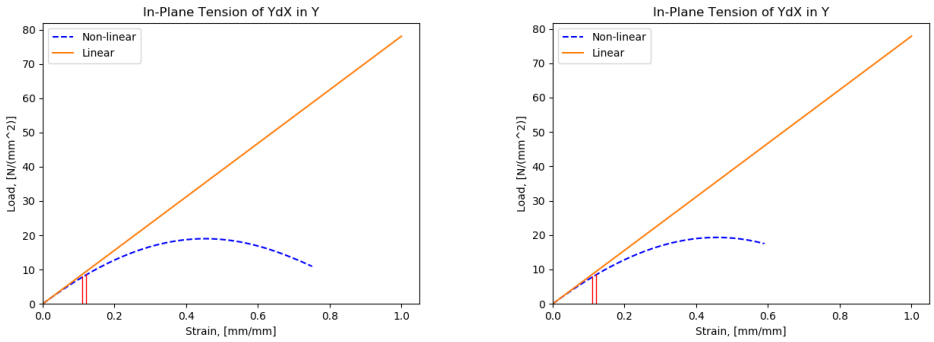

(a)

(b)

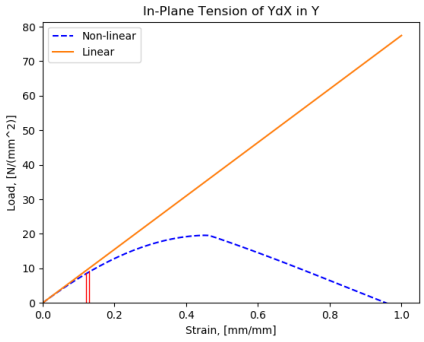

(c)

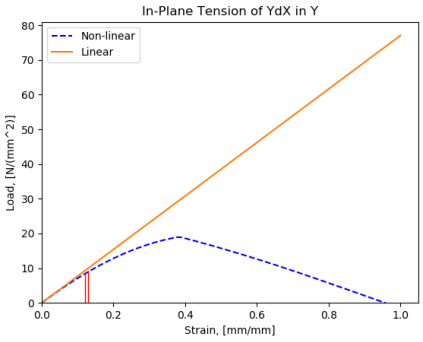

(d)

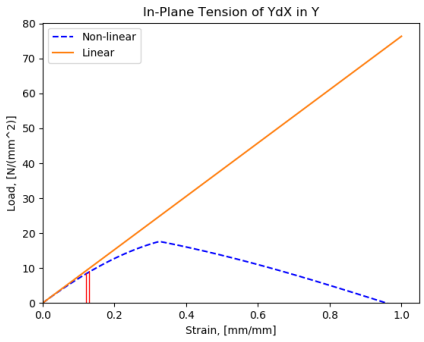

(e)

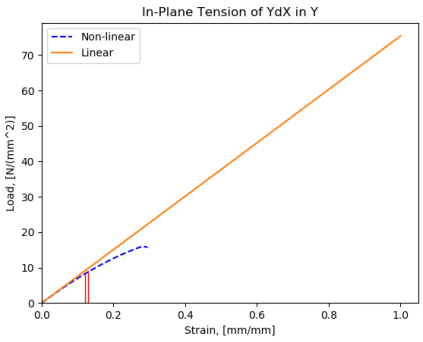

(f)

Figure 43: Results from varying parameter b in the YdX

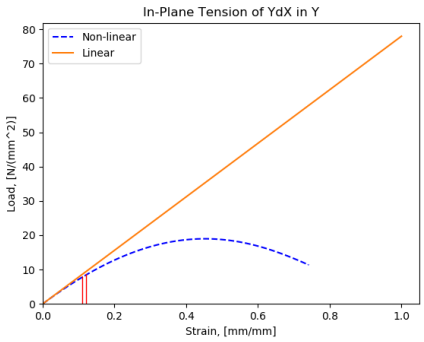

(a)

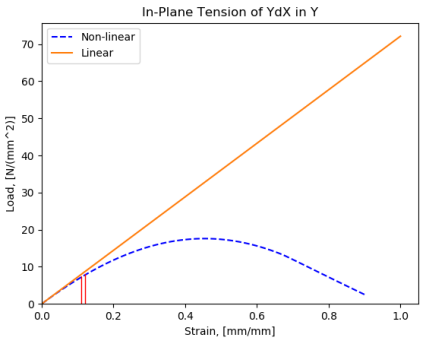

(b)

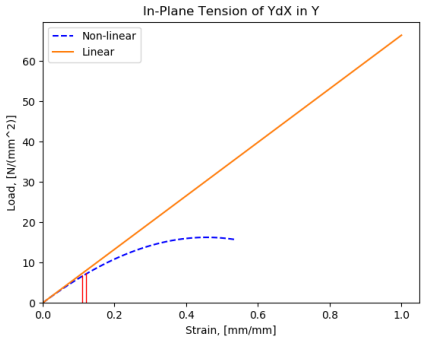

(c)

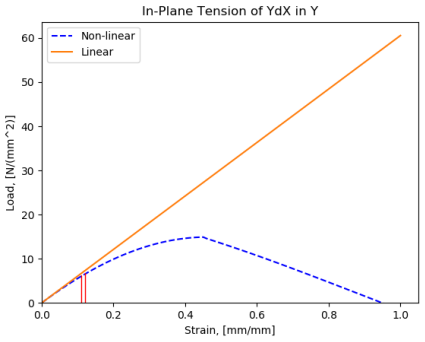

(d)

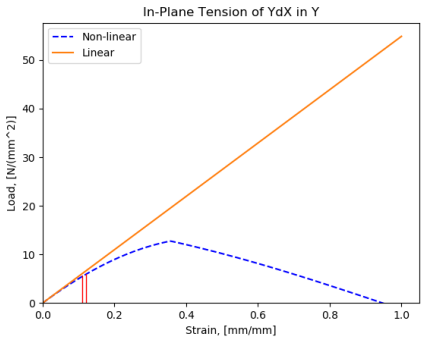

(e)

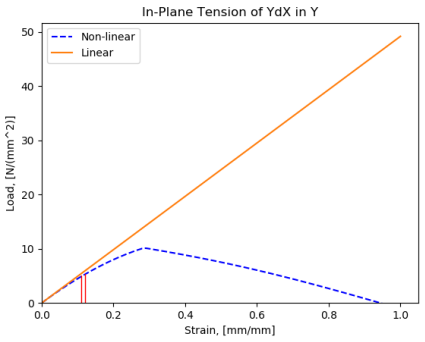

(f)

Figure 44: Results from varying parameter *c* in the YdX

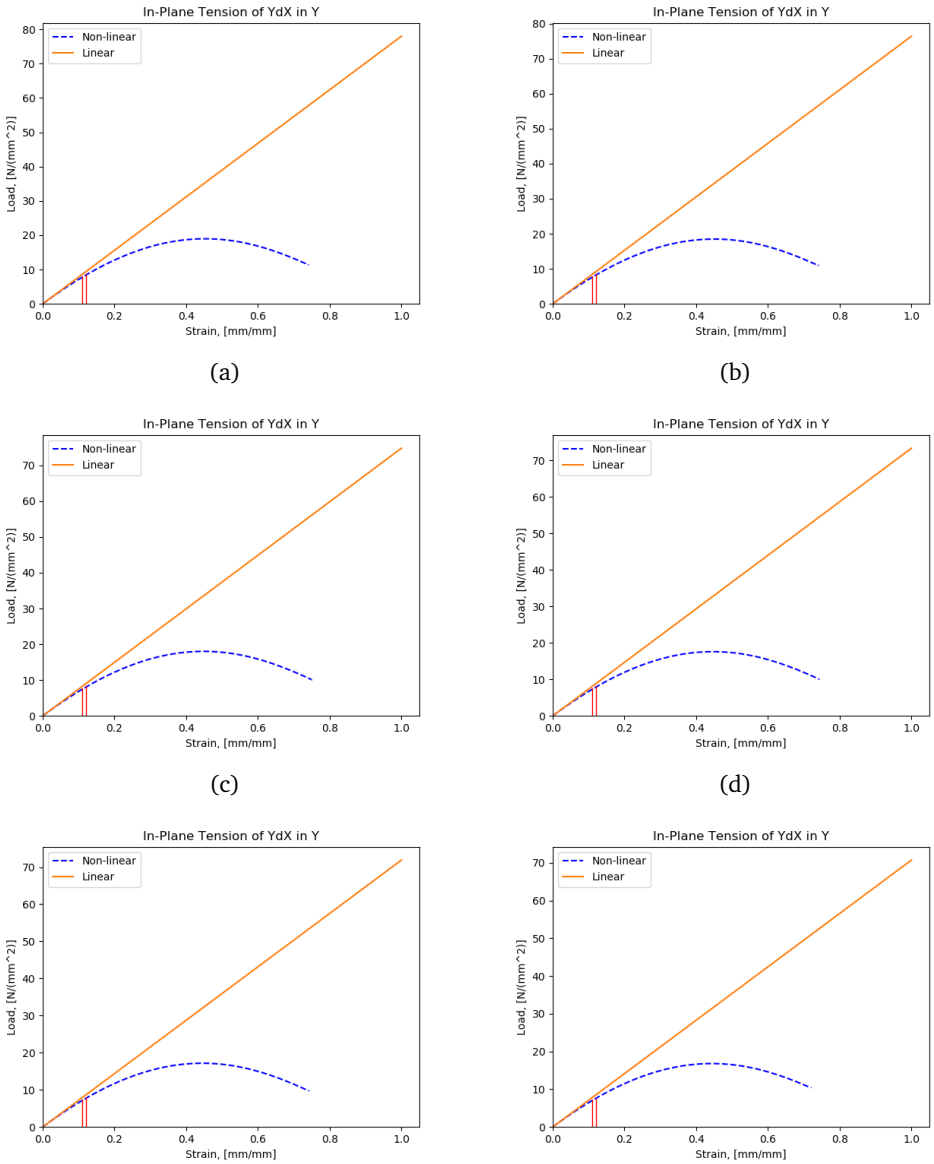

Figure 45: Results from varying parameter *d* in the YdX

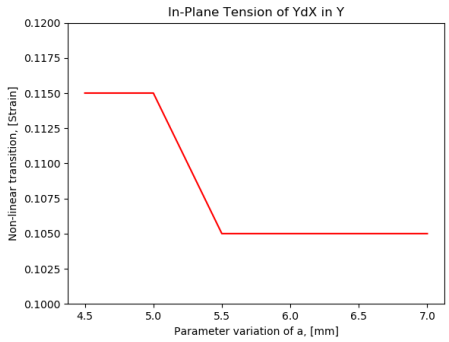

(a)

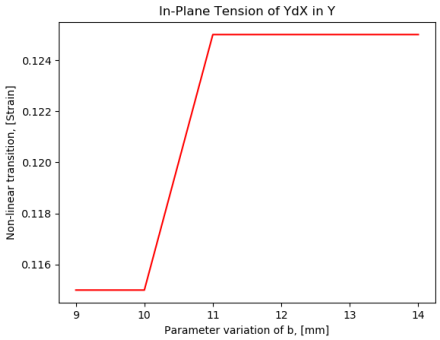

(b)

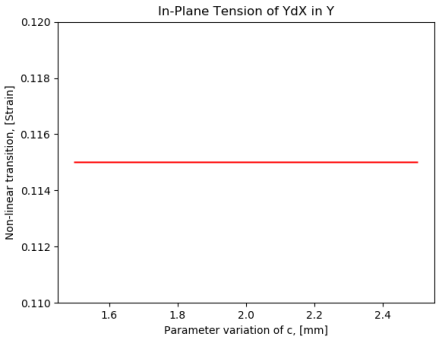

(c)

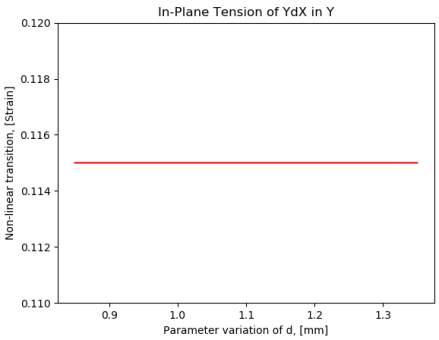

(d)

Figure 46: Plots of the transition values in the YdX for plane tension in Y

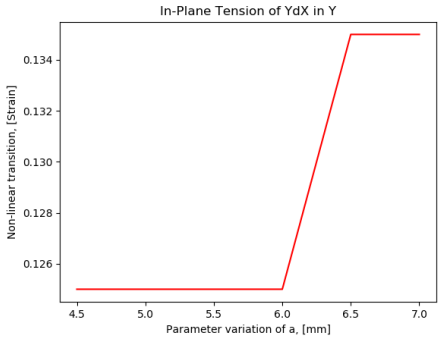

(a)

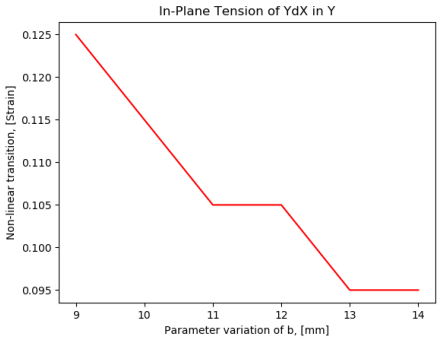

(b)

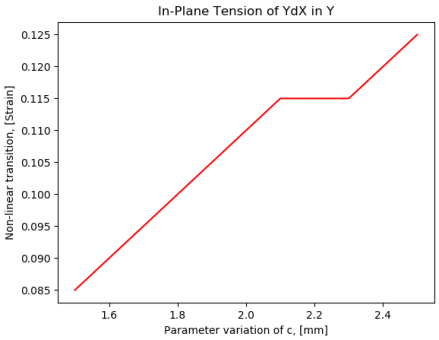

(c)

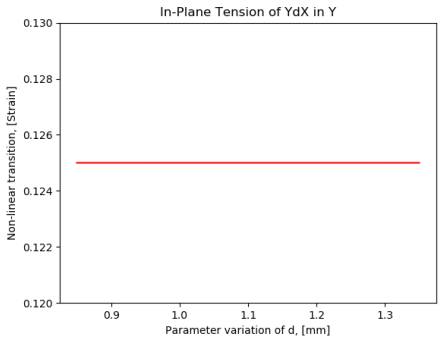

(d)

Figure 47: Plots of the transition values in the YdX for plane tension in Y, unconstrained in XB

Comments on the results

In comparison to in-plane tension of the slits, the YdX plots differ significantly. They show the amount of complexity a flexure pattern could encompass and opens for further analysis. The first thing to notice is the low levels of the transition values. Clearly this unit cell is more prone to geometric non-linearities when subjected to large deformations. However, as in the previous case the transition values does not vary much during the parameter variation.

All the plots show the interesting phenomena of what is referred to as critical points, see section 3.3. For the variation of parameter a and d, the model experiences *buckling* through all the values. Parameters b and c, however, reaches a *bifurcation point* before the limit point is reached for of some values - much like in figure 19b.

The effects of the YdX property of a negative Poisson ratio is not apparent from the results.

The deformation sequence for YdX with in-plane tension are shown in figure 49, and the corresponding plot is shown in figure 48

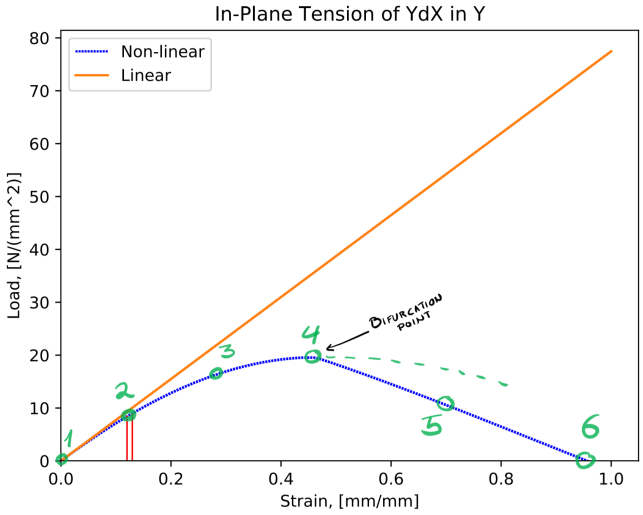

Figure 48: The plot showing the load-strain curve for b = 11 with marked points during the deformation

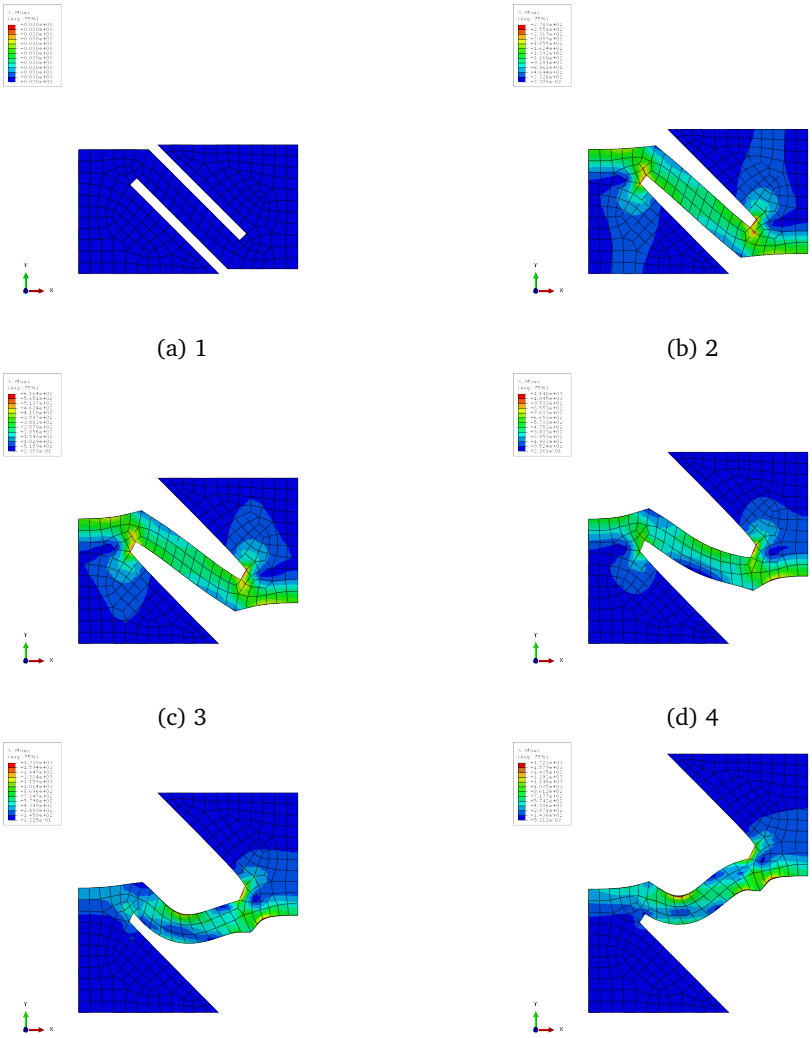

(a) 1 (b) 2

(c) 3 (d) 4

(e) 5 (f) 6

Figure 49: In-plane tension deformation sequence for YdX. The different figures refer to the points marked on figure 48

5.2.2 Cylindrical bending

For this case, the same plots as above have been made for moment versus curvature.

Slits:

In figure 50 and 51, the cylindrical bending deformations of the slits is shown.

Figure 50: Cylindrical bending deformation sequence for Slits 1

Figure 51: Cylindrical bending deformation sequence for Slits 2

The following pages contain plots of the results for cylindrical bending of the slits.

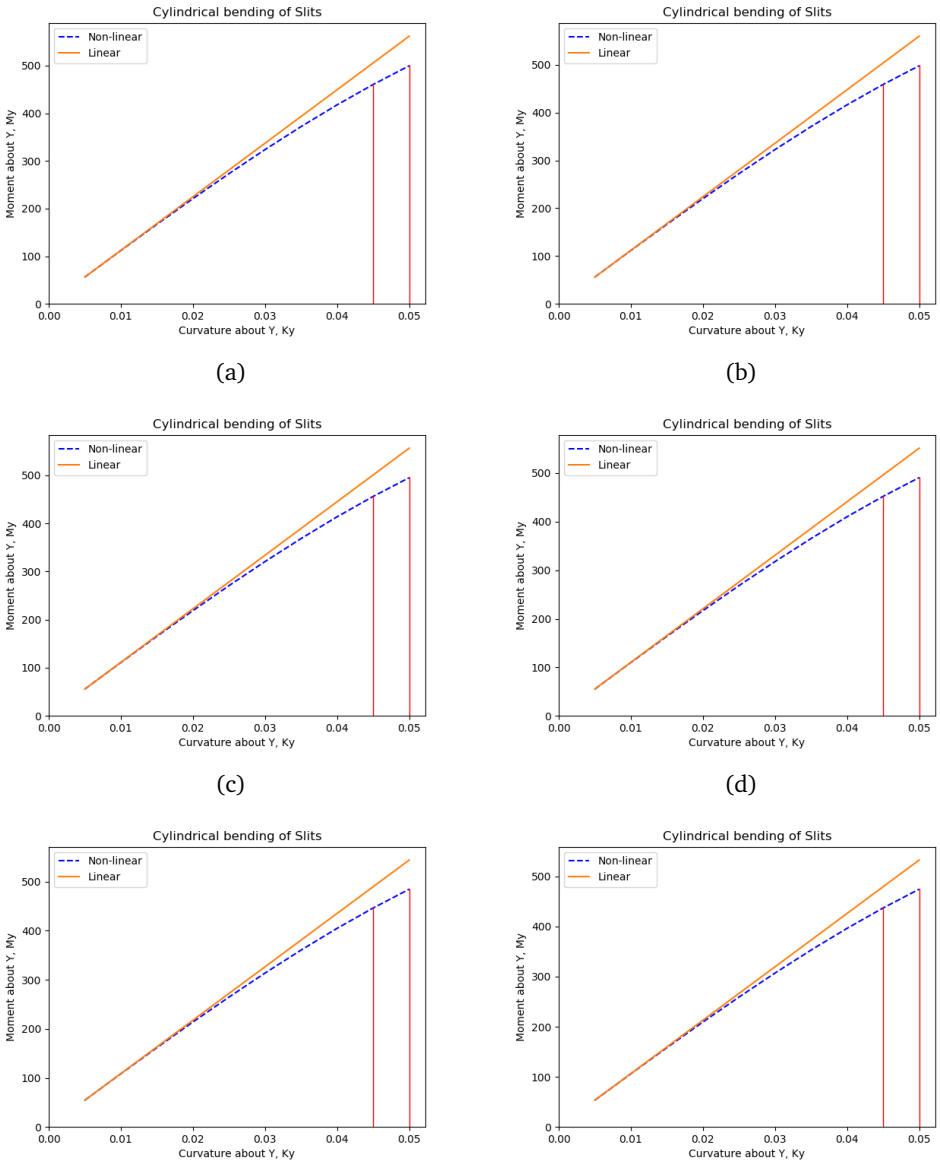

(a) (b)

(c) (d)

(e) (f)

Figure 52: Results from varying parameter a in the Slits

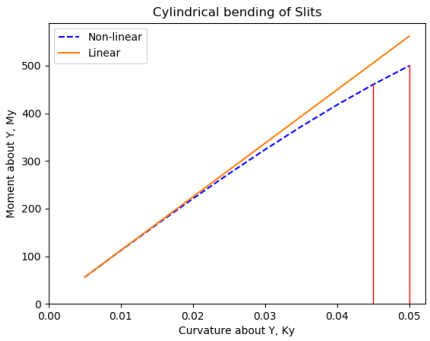

(a)

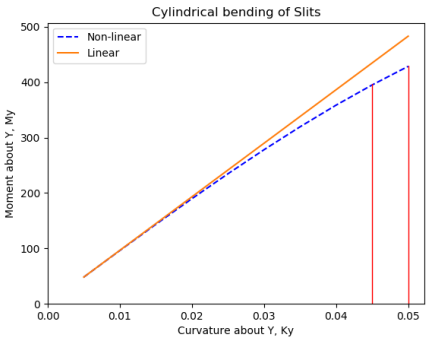

(b)

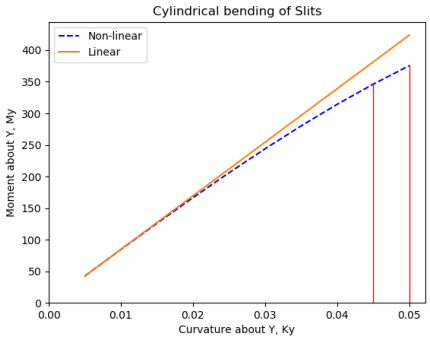

(c)

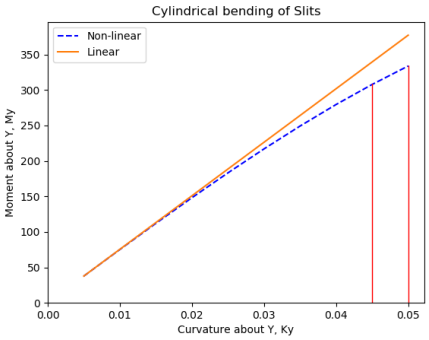

(d)

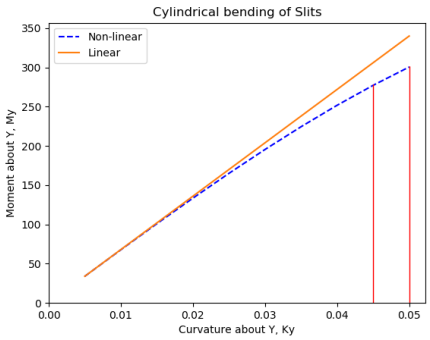

(e)

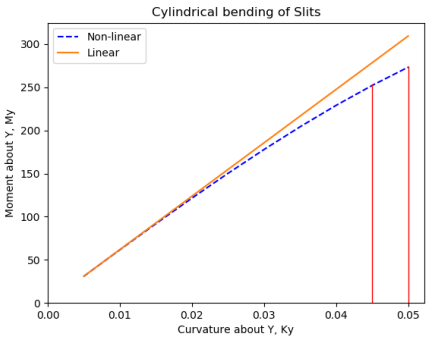

(f)

Figure 53: Results from varying parameter b in the LET

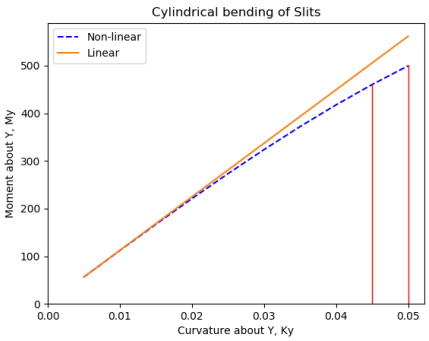

(a)

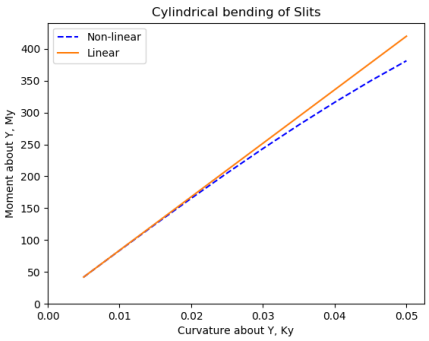

(b)

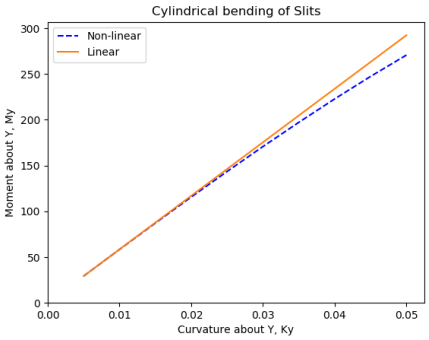

(c)

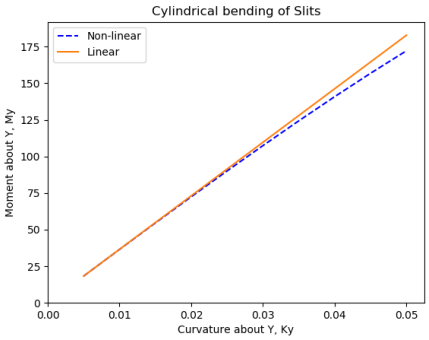

(d)

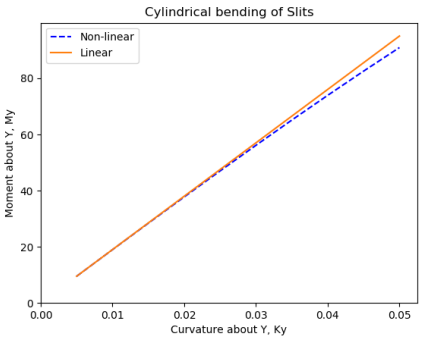

(e)

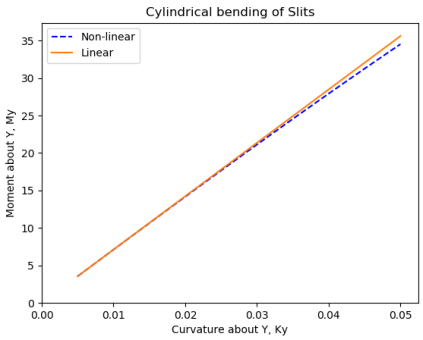

(f)

Figure 54: Results from varying parameter *c* in the Slits

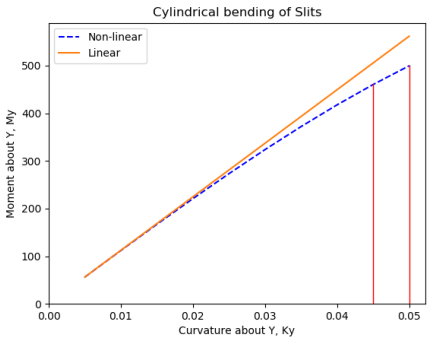

(a)

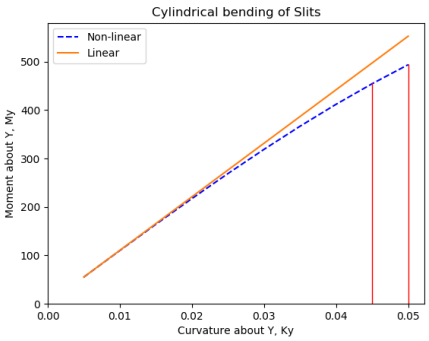

(b)

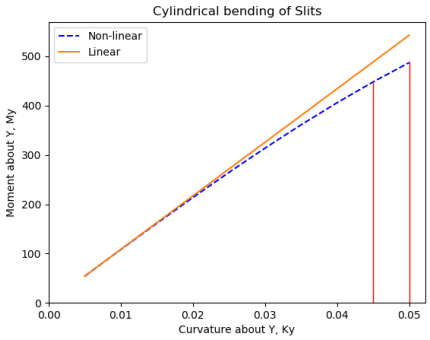

(c)

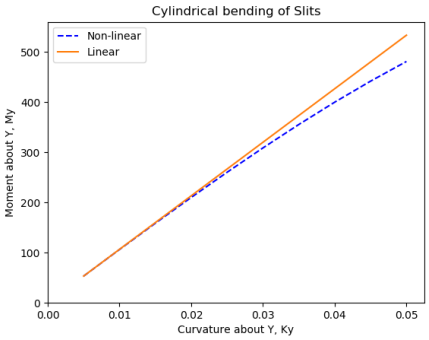

(d)

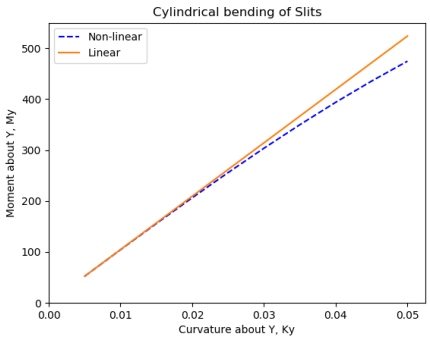

(e)

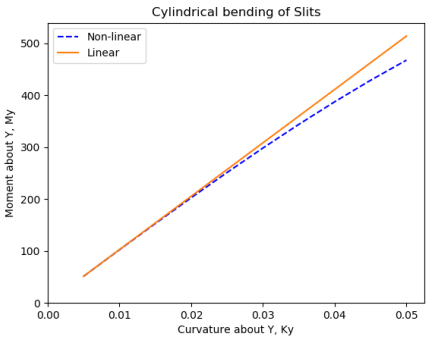

(f)

Figure 55: Results from varying parameter d in the Slits

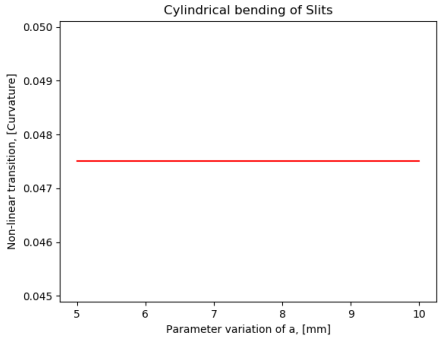

(a)

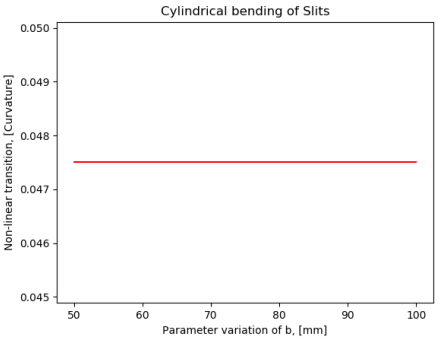

(b)

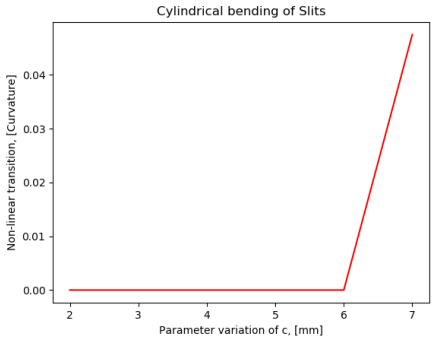

(c)

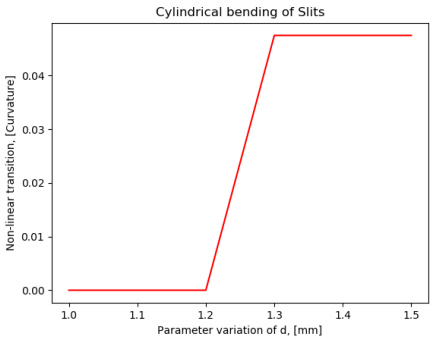

(d)

Figure 56: Plots of the transition values in the Slits for cylindrical bending in Y

Comments on the results

These plots show that during cylindrical bending, the transition value remains quite stable, and is not even reached, for some variations of parameter c and d. This last aspect is interesting, because it meas that the torsion flexure does not contribute as much to the geometric non-linearities as one would think, considering the flexure pattern is being bent down to a radius of only 2 cm.

YdX:

In figure 57 and 58, the cylindrical bending deformations of the YdX is shown.

Figure 57: Cylindrical bending deformation sequence for YdX 1

Figure 58: Cylindrical bending deformation sequence for YdX 2

The following pages contain plots of the results for cylindrical bending of the YdX.

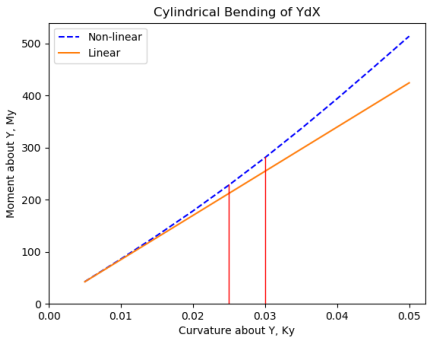

(a)

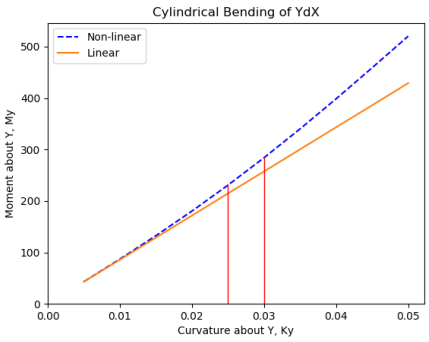

(b)

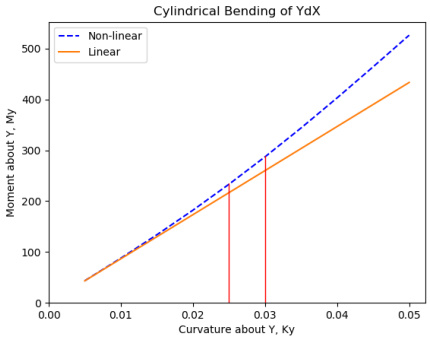

(c)

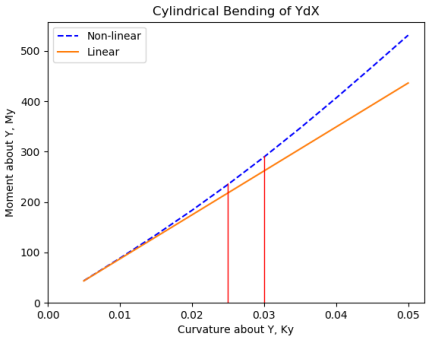

(d)

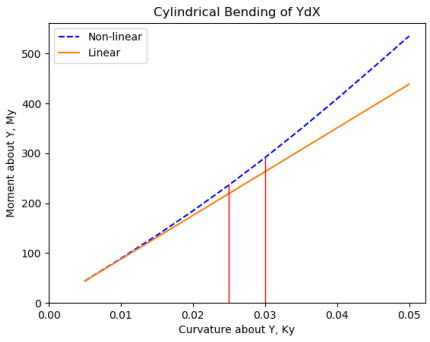

(e)

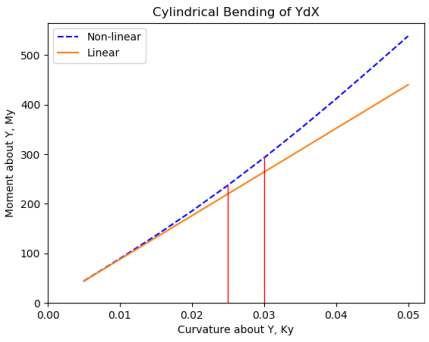

(f)

Figure 59: Results from varying parameter a in the YdX

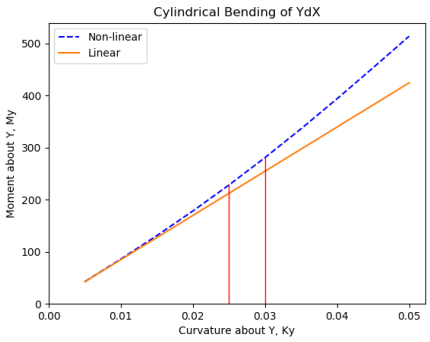

(a)

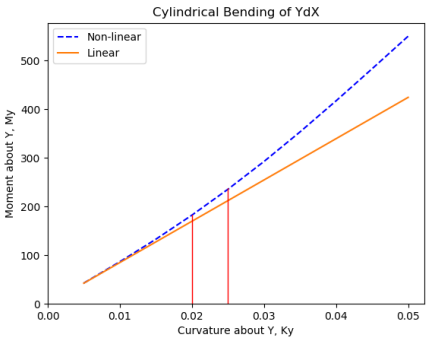

(b)

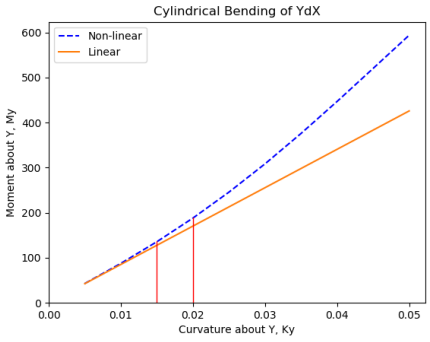

(c)

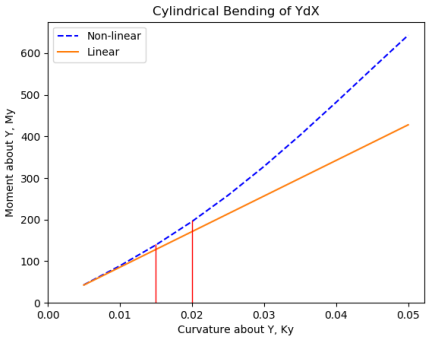

(d)

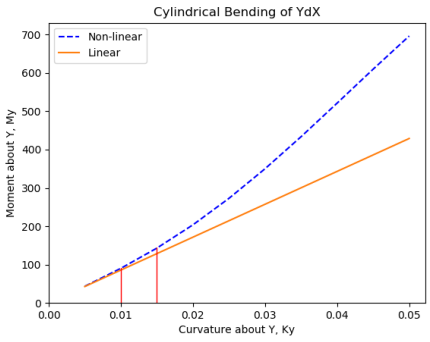

(e)

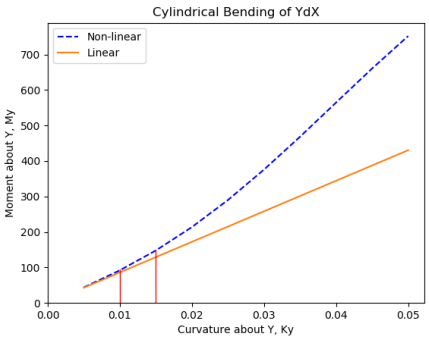

(f)

Figure 60: Results from varying parameter b in the YdX

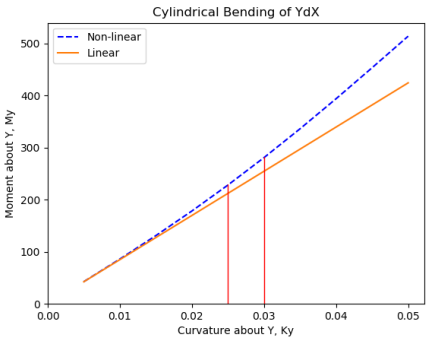

(a)

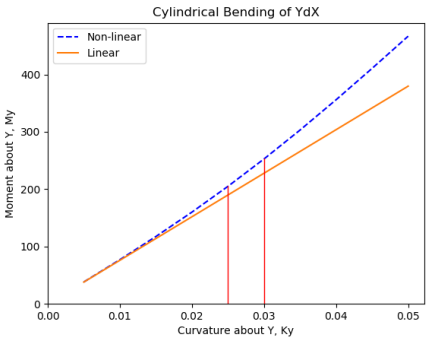

(b)

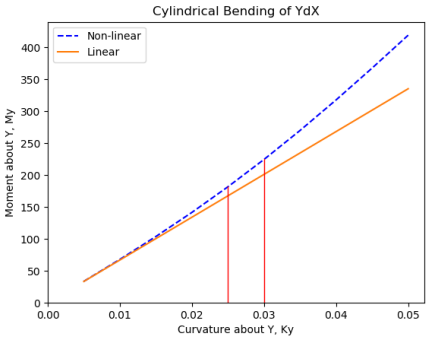

(c)

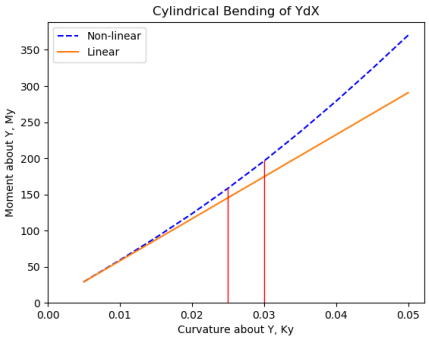

(d)

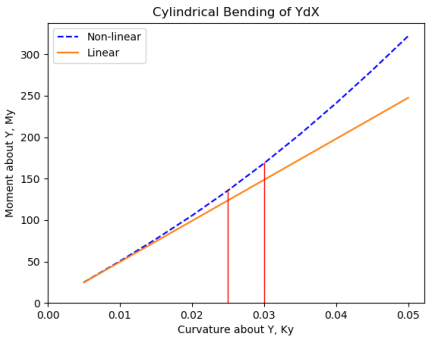

(e)

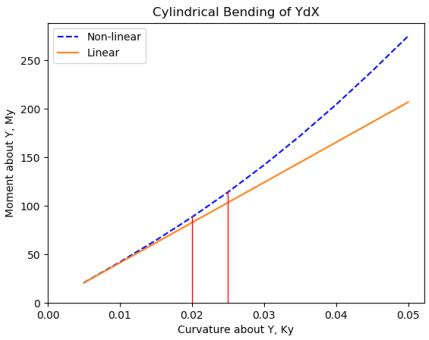

(f)

Figure 61: Results from varying parameter *c* in the YdX

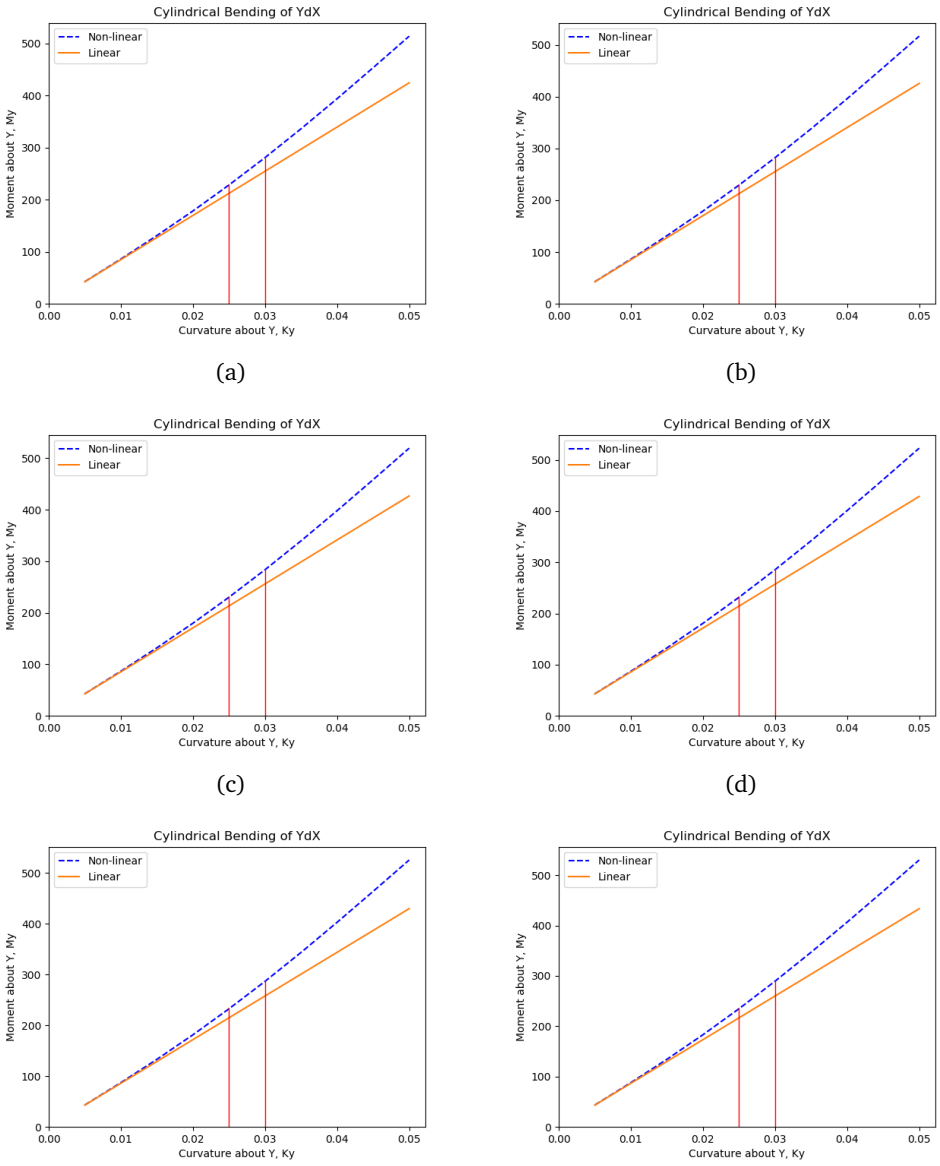

(a) (b)

(c) (d)

(e) (f)

Figure 62: Results from varying parameter d in the YdX

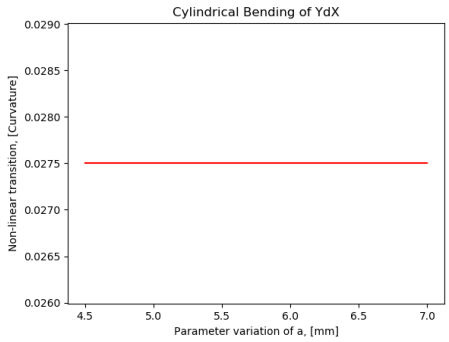

(a)

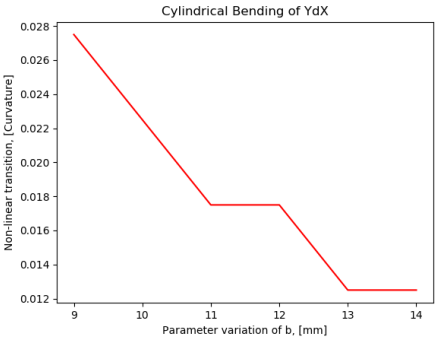

(b)

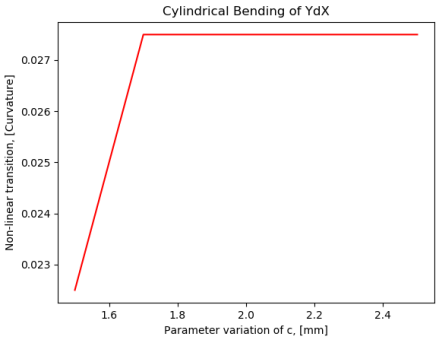

(c)

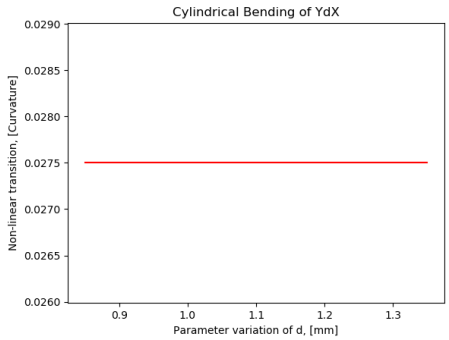

(d)

Figure 63: Plots of the transition values in the YdX for cylindrical bending in Y

Comments on the results

These plots differ from the slits bending plots in that the non-linear curve is increasing rather than showing a softening behaviour. This probably comes from the flexure being at an angle other than orthogonal to the applied moment. This introduces a bending moment in the flexure, which due to the 2nd moment of inertia, adds a greater source of geometric non-linearity, seen in the in-plane tension case. The transition values are lower than in the slits case, but have about the same stability.

It is not clear how to compare the transition value of the bending case to the in-plane tension case. This is something that need further study.

5.3 Contact analysis

The results from the analysis where extracted as the resulting moment at the deformed surfaces and the curvature at the given increment. To calculate the moment, the reaction force in y and z at each node on the surface was probed, and multiplied with the respective arm. The arm was the distance from the probed node to a chosen reference node in the mid surface.

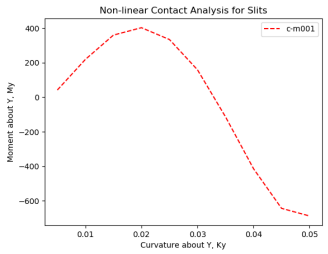

(a) Slits

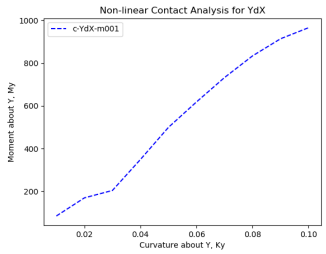

(b) YdX

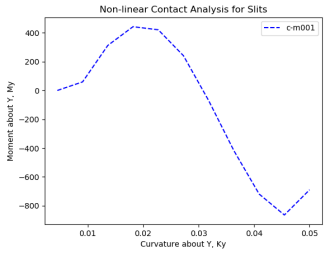

(c) Slits

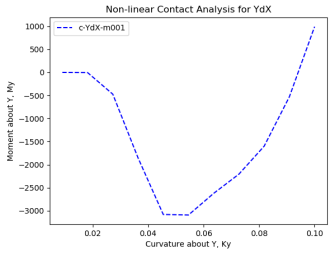

(d) YdX

Figure 64: The contact bending responses

Comments on the results

In figure 64 the plots for the analysis i shown. Plot *a* and *b* show the results from using 10 steps and *c* and *d* from using a single step. There is not much to be interpreted from the plot that could give new insight to the behaviour of the patterns. However, they do provide some information about the bending functions used, presented in section 4.2.5. In a typical contact problem the tangent stiffness of the load curve would abruptly increase when contact was initiated. In the current cases, when contact is reached at about 0.015 curvature, no such change is clearly seen on the plots. Inspection of the output database file(ODB file) from the simulations shows that due to the equations used

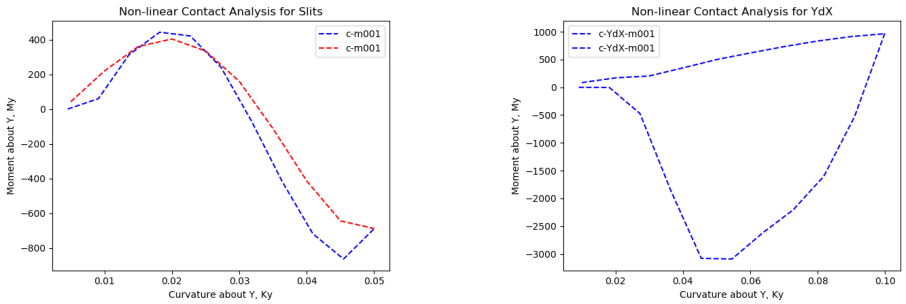

(a) Slits (b) YdX

Figure 65: The contact responses compared

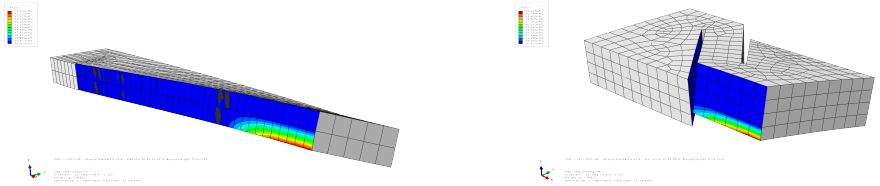

(a) The contact surfaces on the slits (b) The contact surfaces on the YdX

Figure 66: The contact surfaces for the two patterns

to induce the pure moment, large reactions forces emerges in the contact area. These forces are too large because the bending equations are forcing a cylindrical bending on the model. This produces an axial strain component in-plane, which invalidates the assumption of a pure moment load case. The forces coming from this in-plane strain works against the reaction forces from the boundary condition, giving the load curve in the plots. Even though the bending equations was verified in section 4.2.5, they do not hold true when contact is achieved. In figure 67, the reaction force during the contact analysis is shown initially, right before contact and right after contact. In 67c and 67f it can be seen that the RFs from the contact surface cancels out the RFs from the BCs.

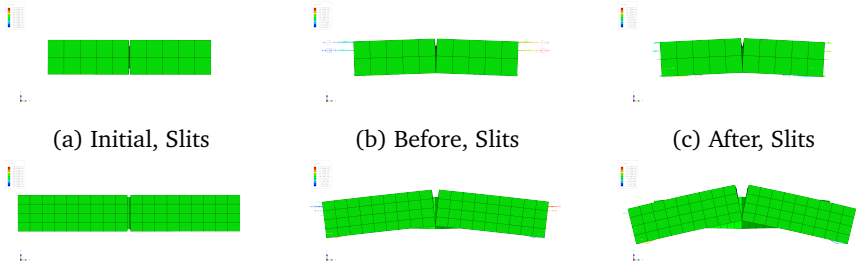

(a) Initial, Slits (b) Before, Slits (c) After, Slits

(d) Initial, YdX (e) Before, YdX (f) After, YdX

Figure 67: The reaction forces at the model boundary for slits and YdX

When performing the contact analysis, the slit in the models had to be reduced to a size of 0.1mm and 0.25mm for the slits and the YdX, respectively. This much smaller than a normal laser cutter is able to cut. However, in real life, contact happens quite easily when bending these two patterns, which means that cylindrical bending an uncommon

load case. A combination of other deformations are apparent, and adds complexity to a contact analysis.

In these two pattern, the contact surfaces was relatively easy to choose. However, in patterns with a different repeating units, e.g with mode cuts, the choice could become harder.

Another issue about this analysis is that the contact area is a source of inertia in the model. The ABAQUS user manual [4] states that during such events the use of static steps should be avoided.

5.4 Idealization error

5.4.1 Laser cutting

In the project work the laser cutter was used to cut the patterns. The strength of the laser cut could be varied by changing the intensity of the beam and how fast it moved along the material. It was observed that cuts made with a single high intensity, slow cut tended to have a draft angle at the cut surfaces(See figure 68). This could be avoided at some extent by performing several, less intensive cuts. The draft angle would probably affect the results of a physical test due the section asymmetry about the mid-plane. This would introduce a B-matrix in the total stiffness matrix, see section 3.1, adding complexion to the stiffness calculation. If this is not compensated for, the results would be invalid.

Figure 68: MDF section after laser cuts of different intensity and speed

5.4.2 Thermal effects

Some materials responds to heat in a way that could cause uncertainties of its properties. The glue that hods the MDF together is probably affected by the intense heat of the laser cutting, causing the material properties presented in section 2.4 to be slightly off.

5.5 To sum up

The results from the analyses have provided some useful insights to the response of the slits pattern and the YdX. Below, some key points are:

- How the geometric non-linearities responds to parameter variation of the base models. It seems that the parameter b is the one most sensitive to change in value during in-plane tension, with respect to geometric non-linearity. This is also the case in cylindrical bending of YdX. No conclusion can be drawn from the slits, due to the stability.
- The different load cases gives unique information about the patterns.
- Adding more load cases is justified by the good results from previous tests.
- A contact analysis is a complex study, and would not be suitable for further parametric studies, as it is very case sensitive

6 Conclusion

This report has, by studying the non-linearities associated with large deformations and contact, contributed to the knowledge of the mechanical behaviour of flexure patterns. To achieve this a numerical parameter study has been performed.

Several script has successfully been written in python to automate the analyses. They have been designed to produce the parts and the load cases, and submitting the jobs in ABAQUS, in addition to read the output values and plot the results from the simulations.

The discovered details on the different non-linear behaviours are listed below.

Geometric non-linearities

A transition value of 10% deviation from the linear curve has been chosen, based on a discussion of the possible applications of the flexure patterns. This value helped to give a reference during the pattern analysis.

Based on the results, it can generally be said that the variation of the non-linear effect from large deformations is small throughout the parametric study.

In the case of in-plane tension, the two patterns differ significantly, due to the different deformation modes the flexures in the repeating unit experiences.

- The *slits pattern* shows less sensitivity towards geometric non-linearities by increasing the height c of the flexure beam.
- The *YdX* experiences highly unstable deformation during in-plane tension, resulting in buckling. These non-linear phenomena poses such an instability that it is recommended to stay well within these strain values. It further justifies the use of a error criteria of 10%, which is relatively far from the critical points.
- The transversely unconstrained cases for the slits pattern indicates a good linear relation well over a unit strain of one, for all the tested parameter values. This shows the importance of the boundary conditions.
- The unconstrained YdX does not show any major differences from the constrained case.
- Variable **b** seems to be the most sensitive to parameter change, with respect to the transition value.

The cylindrical bending case was based on a set of kinematic equations giving a consistent deformation sequence. The curvature for the analyses was chosen to be 0.05, which corresponds to a curvature radius of 2cm:

- The transition values for the slits pattern remained stable, close to the maximum curvature. For the variation of the length of the flexure beam, b, and the parameter a the 10% deviation was not even reached for some values. This result suggests that the torsional response of the flexure deviates insignificantly from a linear approximation.
- The YdX had transition values at about 0.03, and also very stable across the parameter range. It showed a significantly different elastic response than the slits, due to the angled orientation of the flexure beam absorbing the deformation as both

torsion and moment.

Contact

Generally it is found that the contact analysis is very case specific, and from the perspective of performing an automated study, there are several reasons for not pursuing this field of non-linearities:

- The contact analysis requires an exact evaluation of each geometry, and several well justified choices of the contact parameters needs to be made.
- It is a very specific study, and does not quite fit in to a broad parametric study.

It was found, however that the kinematic equations used to produce the cylindrical bending failed on consistency after contact occurred.

6.1 Future Work

This thesis has studied the fundamental cases for two flexure patterns, and several future paths can be suggested to take the work further:

- An key aspect is to make the procedure of the parametric study more generic. This includes to normalize the values used to enable comparison between different results. This could be to normalize curvature on the thickness of the plate or find a way to compare the transition value for strain and curvature
- The deviation value chosen to be 10% in this study, could be further evaluated, and chosen based on different criteria
- Run more parameter test, with different values of a, b, c and d.
- Run parameter analyses based on the ratio between the different parameters, and find the optimal length to height of the flexure beam of slits and YdX for example
- The complexity of the YdX comes mainly from the angled flexure. For this reason, it would be interesting to see how the geometric non-linearities responds to a parameter analysis of the angle.

Bibliography

[1] Howell, L.L., M. Orthoplanar mechanisms. URL: https://compliantmechanisms.byu.edu/content/ortho-planar-spring.

[2] Konaković, M., Crane, K., Deng, B., Bouaziz, S., Piker, D., & Pauly, M. 2016. Beyond developable: computational design and fabrication with auxetic materials. *ACM Transactions on Graphics (TOG)*, 35(4), 1–11. URL: http://delivery.acm.org/10.1145/2930000/2925944/a89-konakovic.pdf?ip=129.241.230.204&id=2925944&acc=ACTIVE%20SERVICE&key=CDADA77FFDD8BE08%2E5386D6A7D247483C%2E4D4702B0C3E38B35%2E4D4702B0C3E38B35&CFID=811875756&CFTOKEN=90054571&__acm__=1505985616_09815f7e5eb9375ef34a7583c4b7bb57, doi:10.1145/2897824.2925944.

[3] Mijares, C. 2018. Nave lamp. URL: https://www.behance.net/gallery/7604137/Lampara-Nave.

[4] Systèmes, D. 2014. Abaqus 6.14 documentation collection. URL: http://abaqus.software.polimi.it/v6.14/index.html.

[5] Østmo, O., Birkeland, S., & Grimstad, E. L. 2017. Behaviour of flexure patterns: Experimental and finite element approach. *Semester project for MTP, NTNU*.

[6] Steinert, M. & Leifer, L. J. 2012. 'finding one's way': Re-discovering a hunter-gatherer model based on wayfaring. *International Journal of Engineering Education*, 28(2), 251.

[7] Howell, L. L., Magleby, S. P., & Olsen, B. M. 2013. *Handbook of compliant mechanisms*. John Wiley & Sons.

[8] Jacobsen, J. O., Howell, L. L., & Magleby, S. P. 2007. Components for the design of lamina emergent mechanisms. URL: http://dx.doi.org/10.1115/IMECE2007-42311, doi:10.1115/IMECE2007-42311.

[9] Jacobsen, J. O., Chen, G., Howell, L. L., & Magleby, S. P. 2009. Lamina emergent torsional (let) joint. *Mechanism and Machine Theory*, 44(11), 2098–2109. URL: http://www.sciencedirect.com/science/article/pii/S0094114X09001116, doi:http://dx.doi.org/10.1016/j.mechmachtheory.2009.05.015.

[10] Nelson, T. G., Lang, R. J., Pehrson, N. A., Magleby, S. P., & Howell, L. L. 2016. Facilitating deployable mechanisms and structures via developable lamina emergent arrays. *Journal of Mechanisms and Robotics*, 8(3), 031006–031006–10. URL: http://dx.doi.org/10.1115/1.4031901, doi:10.1115/1.4031901.

[11] Evans, K. E. & Alderson, A. 2000. Auxetic materials: Functional materials and structures from lateral thinking! *Advanced Materials*, 12(9), 617–628. URL: http:https://doi.org/10.1002/(SICI)1521-4095(200005)12:9<617::AID-ADMA617>3.0.CO;2-3http://onlinelibrary.wiley.com/store/10.1002/(SICI)1521-4095(200005)12:9<617::AID-ADMA617>3.0.CO;2-3/asset/617_ftp.pdf?v=1&t=jaij2502&s=37e00ad08cebb27aa48e173a85f00364ce19c12a, doi:10.1002/(SICI)1521-4095(200005)12:9<617::AID-ADMA617>3.0.CO;2-3.

[12] Körner, C. & Liebold-Ribeiro, Y. 2015. Asystematic approach to identify cellular auxetic materials. *Smart Materials and Structures*, 24(2), 025013. URL: http://iopscience.iop.org/article/10.1088/0964-1726/24/2/025013/pdf, doi:10.1088/0964-1726/24/2/025013.

[13] Herakovich, C. T. 1998. *Mechanics of fibrous composites*. Wiley, New York.

[14] Cook, R. D. 2002. *Concepts and applications of finite element analysis*. Wiley, New York, 4th ed. edition.

[15] Felippa, C. 2017. Nonlinear finite element methods (asen 6107). URL: https://www.colorado.edu/engineering/CAS/courses.d/NFEM.d/Home.html.

[16] Ju, F., Xia, Z., & Zhou, C. 2008. Repeated unit cell (ruc) approach for pure bending analysis of coronary stents. *Computer Methods in Biomechanics and Biomedical Engineering*, 11(4), 419–431. URL: https://doi.org/10.1080/10255840802010454, doi:10.1080/10255840802010454.

Appendices

*

A Documents

A.1 Risk Assessment

ID	27076	**Status**	**Dato**
Risikoområde	Risikovurdering: Helse, miljø og sikkerhet (HMS)	Opprettet	30.01.2018
Opprettet av	Eivind Lystad Grimstad	Vurdering startet	30.01.2018
Ansvarlig	Nils Petter Vedvik	Tiltak besluttet	
		Avsluttet	07.06.2018

Risikovurdering:

Master thesis - non-linear analysis @ Nils Petter Vedvik

Gyldig i perioden:
1/15/2018 - 6/11/2018

Sted:
MTP

Mål / hensikt
Non-Linear Finite Element Analysis of Sheets with Integrated Patterns

Bakgrunn
Master thesis, 10th semester.

Beskrivelse og avgrensninger
Working with simulation software as an analysis tool.
Primarely work done by the desktop.
If a new patterns needs to be made, I will use the laer cutter.

Forutsetninger, antakelser og forenklinger
Does not see any major risks duringany other task than using the laser cutter.

Vedlegg
[Ingen registreringer]

Referanser
[Ingen registreringer]

Oppsummering, resultat og endelig vurdering

I oppsummeringen presenteres en oversikt over farer og uønskede hendelser, samt resultat for det enkelte konsekvensområdet.

Farekilde: **Lasercutter**

Uønsket hendelse: **Dangerous fumes**

Konsekvensområde: Helse — Risiko før tiltak:  Risiko etter tiltak: 

Materielle verdier — Risiko før tiltak:  Risiko etter tiltak: 

Uønsket hendelse: **Damaging the lasercutter**

Konsekvensområde: Materielle verdier — Risiko før tiltak:  Risiko etter tiltak: 

Uønsket hendelse: **Allergic reaction**

Konsekvensområde: Helse — Risiko før tiltak:  Risiko etter tiltak: 

Endelig vurdering

It is not certain that I will use the laser cutter, having used it as enough last semester. I think I have all the patterns I need.

Involverte enheter og personer

En risikovurdering kan gjelde for en, eller flere enheter i organisasjonen. Denne oversikten presenterer involverte enheter og personell for gjeldende risikovurdering.

Enhet /-er risikovurderingen omfatter

- Institutt for maskinteknikk og produksjon

Deltakere

Eivind Lystad Grimstad

Lesere

[Ingen registreringer]

Andre involverte/interessenter

Martin Steinert
Nousha Kheradmand

Følgende akseptkriterier er besluttet for risikoområdet Risikovurdering: Helse, miljø og sikkerhet (HMS):

Helse	Materielle verdier	Omdømme	Ytre miljø
	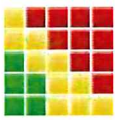	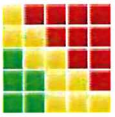	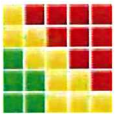

Oversikt over eksisterende, relevante tiltak som er hensyntatt i risikovurderingen

I tabellen under presenteres eksisterende tiltak som er hensyntatt ved vurdering av sannsynlighet og konsekvens for aktuelle uønskede hendelser.

Farekilde	Uønsket hendelse	Tiltak hensyntatt ved vurdering
Lasercutter	Dangerous fumes	HMS-Håndbok
	Damaging the lasercutter	HMS-Håndbok
	Allergic reaction	HMS-Håndbok

Eksisterende og relevante tiltak med beskrivelse:

HMS-Håndbok
[Ingen registreringer]

Risikoanalyse med vurdering av sannsynlighet og konsekvens

I denne delen av rapporten presenteres detaljer dokumentasjon av de farer, uønskede hendelser og årsaker som er vurdert. Innledningsvis oppsummeres farer med tilhørende uønskede hendelser som er tatt med i vurderingen.

Følgende farer og uønskede hendelser er vurdert i denne risikovurderingen:

- **Lasercutter**
  - Dangerous fumes
  - Damaging the lasercutter
  - Allergic reaction

Detaljert oversikt over farekilder og uønskede hendelser:

Farekilde: Lasercutter

Using the lasercutter for manufacturing test specimen.

Uønsket hendelse: Dangerous fumes

Materials can expel fumes when cut. Some fumes can produce corrosive gases when cut.

Årsak: Opening the lid too early

Beskrivelse:

If the lid to the laser cutter is opened too early, fumes from the cutting process has not yet been removed by the fan.

Sannsynlighet for hendelsen (felles for alle konsekvensområder): **Sannsynlig (3)**

Kommentar:

[Ingen registreringer]

Konsekvensområde: Helse

Risiko:

Vurdert konsekvens: **Middels (2)**

Kommentar: The breathing of dangerous fumes could cause issues or irritation in throat

Konsekvensområde: Materielle verdier

Risiko:

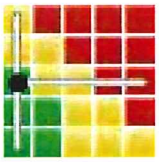

Vurdert konsekvens: **Liten (1)**

Kommentar: [Ingen registreringer]

Uønsket hendelse: Damaging the lasercutter

Not using the equipment properly.

Årsak: Choosing wrong material

Beskrivelse:

Choosing the wrong material when cutting with the laser, could make corrosive gases which can damage the lens of the laser and the nozzle

Sannsynlighet for hendelsen (felles for alle konsekvensområder): **Lite sannsynlig (2)**

Kommentar:

[Ingen registreringer]

Konsekvensområde: Materielle verdier

Risiko:

Vurdert konsekvens: **Svært stor (4)**

Kommentar: [Ingen registreringer]

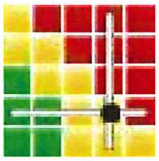

Uønsket hendelse: Allergic reaction

Exposure to the materials over a long period of time may produce allergic reactions.

Årsak: Handeling of material

Beskrivelse:

If the material is beein touched and handeled too much

Sannsynlighet for hendelsen (felles for alle konsekvensområder): **Svært lite sannsynlig (1)**

Kommentar:

[Ingen registreringer]

Konsekvensområde: Helse

Risiko:

Vurdert konsekvens: **Stor (3)**

Kommentar: An allergic reaction could occur,

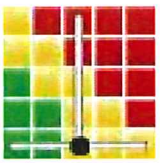

Oversikt over besluttede risikoreduserende tiltak:

Under presenteres en oversikt over risikoreduserende tiltak som skal bidra til å reduseres sannsynlighet og/eller konsekvens for uønskede hendelser.

Detaljert oversikt over besluttede risikoreduserende tiltak med beskrivelse:

Detaljert oversikt over vurdert risiko for hver farekilde/uønsket hendelse før og etter besluttede tiltak

A.2 What is a flexure pattern?

This definition has been written by Oddvin Østmo

The term *flexure pattern* is used in this thesis for the concept of introducing specific cuts in a plate in order to reduce the resistance to bending and stretching. The most characteristic property of a flexure pattern is the ability to make a flexible surfaces from a hard material. The concept appeared first in various *Maker Spaces* and home at hobbyists with access to a laser cutter and has been around for a few years.

It is emphasized that this thesis *introduces the definition of flexure patterns* as it is a term invented by the author and his co-authors from the project thesis in the autumn of 2017. A review of other terms like *living hinge, lattice hinge, kerf bend* and *compliant array* is also used for the same concept.

In order to develop a language to describe the different elements of a flexure pattern precise, we define what we mean by it and what its different constituents.

Flexure pattern is characterized as a 2 dimensional metamaterial that consists of flexures configured in a pattern that increase the compliance compared to the bulk material. The flexures are patterned onto the plane according to a set of rules.

The basic building block of a flexure pattern is the *flexure*. It is a flexible member that is engineered to be compliant in some DOFs. It rely on elastic deformation like bending and torsion to achieve larger travel distances than what is achieved through tensile or compression. A *flexure region* is the part of a flexure pattern that consists of a flexure or a configuration of flexures. The flexure region is engineered to be compliant and is responsible for most of the increased travel distances found in a flexure pattern. A *rigid region* is the rigid part of a flexure pattern where flexures meet to form a joint or a larger area of the flexure pattern where no flexures are present.

The term *pattern* is defined as: a combination of qualities, acts, tendencies, etc., forming a consistent or characteristic arrangement(...). When speaking of a *periodic flexure pattern* one can define the elements for patterning the plane through two non-parallel vectors: the unit of the pattern and the prototile. The *unit of the pattern* corresponds to the least area that preserves all symmetries of the pattern when translated under the two non-parallel vectors. The unit of the pattern is defined independently of the flexure configuration and can sometimes seem a bit odd when describing the flexure pattern. A better method for describing a repeating region of a pattern is by the *prototile*. This correspond to the tile or set of tiles that capture the whole flexure configuration as a continuous piece and can be used to tile the plane though a translation in two directions.

B Codes

The codes that have been made during the semester is added as a ZIP-file delivered with this thesis.